Nuclear Physics **A513** (1990) 125-173
North-Holland

ALIGNMENT PROCESSES AND SHAPE VARIATIONS IN ^{184}Pt

M.P. CARPENTER[1], C.R. BINGHAM, L.H. COURTNEY, V.P. JANZEN[2], A.J. LARABEE[3], Z.-M. LIU[4], L.L. RIEDINGER and W. SCHMITZ[5]

Department of Physics, The University of Tennessee, Knoxville, TN 37996-1200, USA

R. BENGTSSON[6], T. BENGTSSON[6], W. NAZAREWICZ[7] and J.-Y. ZHANG[8]

Joint Institute for Heavy Ion Research, Oak Ridge National Laboratory, Oak Ridge, TN 37831, USA

J.K. JOHANSSON, D.G. POPESCU[9] and J.C. WADDINGTON

McMaster University, Hamilton, Ontario, Canada L8S 4K1

C. BAKTASH, M.L. HALBERT, N.R. JOHNSON, I.Y. LEE and Y.S. SCHUTZ*

Holifield Heavy Ion Research Facility, Oak Ridge National Laboratory, Oak Ridge, TN 37831, USA

J. NYBERG**, A. JOHNSON and R. WYSS

Manne Siegbahn Institute of Physics, Frescativägen 24, S-10405 Stockholm, Sweden
and
Physics Department I, The Royal Institute of Technology, S-10044 Stockholm, Sweden

J. DUBUC, G. KAJRYS, S. MONARO and S. PILOTTE[2]

Université de Montréal, Montréal, P.Q., Canada H3C 3J7

K. HONKANEN† and D.G. SARANTITES

Washington University, St. Louis, MO 63130, USA

D.R. HAENNI

Cyclotron Institute, Texas A&M University, College Station, TX 77843-3366, USA

Received 27 September 1989

Abstract: High-spin states in the transitional nucleus ^{184}Pt were populated via the reactions ^{154}Sm(^{34}S, 4n)^{184}Pt and ^{172}Yb(^{16}O, 4n)^{184}Pt. The yrast band was extended up to $I = 28\hbar$ and six new side bands built on both neutron and proton quasiparticle configurations were observed. Shell correction-type calculations indicate variations of the nuclear shape in different bands, especially as a result of band crossings due to the process of angular momentum alignment. Comparison of

[1] Present address: Argonne National Laboratory, Physics Division, Argonne, IL 60439, USA.
[2] Present address: Chalk River Nuclear Laboratories, Chalk River, Ontario, Canada K0J 1J0.
[3] Present address: TRIUMF, Vancouver, B.C., Canada V6T 2A3.
[4] Permanent address: Lanzhou University, Lanzhou, People's Republic of China.
[5] Present address: Institut für Strahlen und Kernphysik, Nussallee 14-16, D-5300 Bonn 1, Fed. Rep. Germany.
[6] Permanent address: Department of Mathematical Physics, Lund Institute of Technology, S-22100 Lund, Sweden.
[7] Permanent address: Institute of Physics, Warsaw Institute of Technology, PL-00662 Warsaw, Poland.
[8] Permanent address: Institute of Modern Physics, Lanzhou, People's Republic of China.
[9] Present address: Dept. of Nuclear Physics, Australian National University, Canberra, Australia.
* Present address: GANIL Laboratory, B.P. 5027, F-14021 Caen Cedex, France.
** Present address: Niels Bohr Institute, Tandem Accelerator Laboratory, Roskilde, Denmark.
† Department of Physics, University of Jyväskylä, SF-40100 Jyväskylä 10, Finland. Deceased 1987.

the band characteristics are made between ^{184}Pt and eight adjacent nuclei. The pattern of band crossings in these nine nuclei is considered from the viewpoint of blocking comparisons and of theoretical calculations. The competition between low-frequency $\nu i_{13/2}$ and $\pi h_{9/2}$ band crossings is discussed.

E NUCLEAR REACTION ^{154}Sm(^{34}S, 4n), $E = 163$ MeV; ^{172}Yb(^{16}O, 4n), $E = 91$ MeV; measured E_γ, I_γ, $\gamma(\theta)$, $\gamma\gamma$-coin. ^{184}Pt deduced levels, J, π, γ-branching. Enriched targets, array of Compton-suppression Ge detectors. Total routhian surface calculations.

1. Introduction

Shape coexistence, where structures associated with both prolate and oblate shapes are observed within the same nucleus, has been established in the light Pt–Hg nuclei at the upper end of the rare-earth region. These nuclei are referred to as transitional, because they lie in a region between the well-deformed prolate nuclei in the rare-earth region and the slightly to moderately deformed oblate Hg and Pt nuclei at $N > 108$. The shape coexistence is an indication that the cores of these nuclei are "soft" with respect to deformation. One can thus expect significant changes in the nuclear shape to be caused by aligned quasiparticles at high spins [1]). This paper reports on measurements of high-spin states in ^{184}Pt, which lies near the center of this transitional region. While the existence of structures built on prolate and oblate shapes has been previously discussed [see ref. [2]) and references therein], the present work examines with even greater sensitivity the effects of aligned quasiparticles on the nuclear shape.

Earlier measurements of high-spin states in ^{185}Au ($N = 106$) led to the conclusion that there are two major rotational alignment processes, due to $\nu i_{13/2}$ and $\pi h_{9/2}$ quasiparticles, which occur at nearly degenerate rotational frequencies around $\hbar\omega \approx 0.26$ MeV [ref. [3])]. Our initial interpretation of the results on ^{184}Pt (see for example ref. [4])) supported this proposal, and we concluded that both the neutron and proton alignments were responsible for the observed single upbend in the yrast band. Subsequent high-spin measurements on the Ir–Au nuclei at $N = 106$–108 have given support to the proposal that $\pi h_{9/2}$ quasiparticles may align below $\hbar\omega \approx$ 0.35 MeV in this region. However, the new data have also indicated that it is not always possible to determine what alignment processes are occurring in specific bands in these nuclei.

In this paper, we re-examine our previous interpretation of the yrast band in ^{184}Pt by comparing our data with the systematics of the region. We also investigate the polarizing effects aligned high-j quasiparticles have on the nuclear deformation for the rotational bands in ^{184}Pt. Conclusions about the dependence of the shape on these alignments come from a comparison of our spectroscopic data with the results of a set of total routhian surface (TRS) calculations, which are performed utilizing the shell correction method described in ref. [5]). These calculations permit a determination of the shape parameters as a function of rotational frequency and quasiparticle

configuration. The results of this analysis combined with our measurements on the high-spin states in ^{184}Pt have yielded the following important features:

(i) an extension of the yrast band beyond the upbend up to $I = 28\hbar$, demonstrating an alignment gain of $10\hbar$ in the yrast crossing(s);

(ii) the observation and identification of six new side bands built on both proton and neutron quasiparticle configurations;

(iii) predicted nuclear deformation parameters, extracted from the TRS calculations, before and after the band crossing(s) in both the yrast and two quasiparticle bands, exhibiting a variety of configuration-dependent shapes for ^{184}Pt.

(iv) two different scenarios for the interpretation of the band crossings observed in ^{184}Pt and neighboring nuclei. The difference lies in whether certain band crossings are due to proton $h_{9/2}$ or neutron $i_{13/2}$ alignment.

2. Experiment

Measurements of high-spin states in ^{184}Pt were performed at two accelerators. The first was done at the Holifield Heavy Ion Research Facility where high-spin states were populated via the ^{154}Sm(^{34}S, 4n)^{184}Pt reaction at 163 MeV using a stacked target consisting of two 500 μg/cm^2 foils. Gamma-ray coincidences were measured using seven Ge detectors placed at various angles throughout the Spin Spectrometer. Six of these detectors were surrounded by NaI Compton-suppression shields. The remainder of the spectrometer held 64 NaI detectors whose primary function was to act as a total energy and multiplicity filter. The second experiment was performed at the McMaster University Tandem Accelerator Laboratory utilizing the ^{172}Yb(^{16}O, 4n)^{184}Pt reaction at 91 MeV. An array of eight Ge detectors and six NaI counters was used to collect the γ-ray coincidence information. Accepted events consisted of coincidences between at least three Ge detectors or at least two Ge detectors and one NaI detector.

A separate experiment was performed to measure the angular distributions of γ-rays within ^{184}Pt with respect to the beam axis, using five Ge detectors placed at θ-angles 0°, 30°, 45°, 60° and 90°. An accepted event consisted of at least a single Ge detector in coincidence with the NaI multiplicity filter located in the McMaster spectrometer. With the NaI counter geometry used for angular distribution measurements, angular correlations between the Ge detectors and multiplicity filter are small since the detectors which comprise the filter are positioned symmetrically around the beam axis.

2.1. ANGULAR DISTRIBUTION DATA

The detector coincidence efficiencies were properly renormalized by calculating the expected angular intensities for five strong E2 transitions in ^{184}Pt (272.8, 362.4, 432.3, 476.2 and 497.6 keV). The theoretical values for A_2/A_0 and A_4/A_0 were calculated by assuming a value for $\sigma/J = 0.30$ for all five transitions. Pilotte [6]) has

measured the σ/J values in an angular distribution measurement on ^{185}Pt and has found that this ratio remains constant at 0.25 over the decay of the yrast band. Since the reaction used in that measurement [^{174}Yb(^{16}O, 5n)^{185}Pt at 90 MeV] was almost identical to the reaction utilized for the ^{184}Pt angular distribution experiment, our assumption of a constant σ/J for the above transitions is a valid approximation to the data. The solid-angle corrections (Q_2 and Q_4) were also determined and included in the calculations of $W(\theta)$. Once the theoretical values for $W(\theta)$ were found, a correction factor for each angle was determined for the five transitions by renormalizing the experimental angular distributions so that they agree with the theoretical values. A single correction factor was then determined for each angle by averaging over the separate E2 normalization constants.

Table 1 lists the experimental A_2/A_0 and A_4/A_0 coefficients which were determined by a least-squares fit to the experimental intensities. The peak intensities are also given and were measured relative to the $4^+ \rightarrow 2^+$ transition in the yrast band of ^{184}Pt, using the calculated A_0 coefficients from the fitted angular distribution data. However, when multiplets prevented the determination of the intensity of certain transitions, gated spectra from the coincidence experiment were used, comparing the intensities of the peaks of interest with one whose intensity relative to the $4^+ \rightarrow 2^+$ transition was already known. In this table (as well as in the level scheme) spin and/or parities whose assignments are uncertain have been enclosed in parentheses. If the placement of a transition in the level scheme is not absolutely certain, it has been dashed in the level scheme.

When we calculate the absolute intensity for the transitions by including the decays which should occur via internal conversion, the intensities going into most levels balance well with the intensities leaving the levels. An important exception to this agreement is the intensity balance of the isomeric level at 1843.8 keV (8^-) (see the level scheme in fig. 1). While we were unable to measure the intensity of the 613.5 keV transition, we can estimate the maximum intensity which feeds into the 1230.3 keV level (8^+) by comparing the intensity differences of the yrast transitions in and out of this level which should put an upper limit on the intensity of 613.5 keV transition. This intensity can only account for approximately half of the intensity observed feeding into the 1843.8 keV level. This missing intensity is accounted for by 49 and 112 keV transitions from the 1843.8 keV level to the 1793.7 keV (6^-) and the 1730.1 keV (7^+) levels, respectively. These transitions were not observed in our measurements but were reported by Burde *et al.*[7]) as accounting for the other half of the intensity out of the 1843.8 keV level.

2.2. LEVEL SCHEME ASSIGNMENTS

Several previous studies had established the low-energy level structure of ^{184}Pt utilizing both radioactive decay and heavy-ion reactions. Burde *et al.*[7]) were the

TABLE 1

Angular distribution data for ^{184}Pt

E_γ [keV]	I_γ	A_2/A_0	A_4/A_0	Assignment	Assigned multipolarity
118.1	2.0 (2)	−0.90 (28)	0.24 (21)	$6^- \rightarrow 5^-$	E2/M1
121.0	1.5 (2)	−0.61 (44)	−0.05 (33)	$7^- \rightarrow 6^-$	E2/M1
154.6 [b])	1.4 (3)			$8^- \rightarrow 7^-$	
160.0 [b])	1.6 (4)			$9^- \rightarrow 8^-$	
162.8 [a])	64.0 (4)			$2^+ \rightarrow 0^+$	
172.9 [c])				$11^- \rightarrow 10^-$	
177.7	5.8 (1)	−0.86 (04)	0.05 (30)	$9^- \rightarrow 8^-$	E2/M1
198.7	6.6 (1)	−0.60 (03)	0.05 (03)	$10^- \rightarrow 9^-$	E2/M1
218.8 [b])	3.3 (4)			$11^- \rightarrow 10^-$	
221.0 [a])	0.7 (2)			$10^- \rightarrow 9^-$	
238.0	2.4 (1)	−0.84 (05)	0.09 (05)	$12^- \rightarrow 11^-$	E2/M1
239.5	2.3 (1)	0.15 (04)	0.05 (05)	$7^- \rightarrow 5^-$	E2/M1
254.5	1.7 (3)	−0.56 (12)	0.07 (10)	$13^- \rightarrow 12^-$	E2/M1
269.3	3.4 (2)	−0.53 (14)	0.08 (11)	$14^- \rightarrow 13^-$	E2/M1
272.8	100.0 (3)	0.34 (01)	−0.12 (01)	$4^+ \rightarrow 2^+$	E2
278.6	2.2 (2)	−0.51 (20)	0.34 (17)	$15^- \rightarrow 14^-$	E2/M1
281.1	2.7 (2)	0.12 (25)	0.11 (13)	$8^- \rightarrow 6^-$	E2
286.7	1.0 (1)	−0.26 (13)	−0.04 (14)	$12^- \rightarrow 11^-$	E2/M1
287.4	1.6 (1)	−0.96 (07)	0.25 (07)	$16^- \rightarrow 15^-$	E2/M1
290.2	1.4 (1)	−0.80 (08)	−0.02 (08)	$17^- \rightarrow 16^-$	E2/M1
298.8 [c])				$18^- \rightarrow 17^-$	
303.4	2.7 (1)	0.36 (05)	0.00 (06)	$18^{(+)} \rightarrow 18^+$	E2/M1
304.6	1.3 (1)	−0.29 (11)	−0.07 (11)	$19^- \rightarrow 18^-$	E2/M1
314.3 [b])	3.4 (3)			$(16^+) \rightarrow 16^+$	
314.7 [b])	7.4 (3)			$9^- \rightarrow 7^-$	
320.5 [a])	0.5 (1)			$(20^-) \rightarrow 19^-$	
322.7	1.1 (1)	0.67 (16)	−0.08 (16)	$20^{(+)} \rightarrow 20^+$	E2/M1
344.3 [a])	1.1 (1)			$(22^+) \rightarrow 22^+$	
345.3 [b])	2.3 (4)	0.43 (08)	0.12 (09)	$15^- \rightarrow 13^-$	E2
355.1 [b])	1.5 (5)			$13^- \rightarrow 14^+$	
358.6 [b])	5.4 (9)	0.33 (08)	0.03 (07)	$15^- \rightarrow 13^-$	E2
362.4	90.0 (4)	0.36 (01)	−0.09 (01)	$6^+ \rightarrow 4^+$	E2
375.7 [b])	3.3 (9)			$10^- \rightarrow 8^-$	
376.4 [b])	4.4 (3)			$10^- \rightarrow 8^-$	
388.4 [b])	4.2 (4)			$(11^-) \rightarrow 12^+$	
390.0 [a])	1.5 (5)			$4^+ \rightarrow 2^+$	
393.8	7.0 (1)	0.23 (03)	−0.09 (03)	$11^- \rightarrow 9^-$	
417.8	4.6 (1)	0.24 (03)	0.16 (03)	$11^- \rightarrow 9^-$	E2
424 [a])	1.5 (2)			$7^+ \rightarrow 5^+$	
432.3	91.7 (4)	0.32 (01)	−0.08 (01)	$8^+ \rightarrow 6^+$	E2
441.2	5.4 (2)	−0.37 (07)	−0.15 (08)	$5^- \rightarrow 4^+$	E1
456.8 [a])	4.8 (3)			$12^- \rightarrow 10^-$	
457.6 [b])	2.6 (7)			$13^- \rightarrow 11^-$	
459.5	4.3 (1)	0.38 (06)	−0.11 (06)	$12^- \rightarrow 10^-$	E2
461.9	16.3 (2)	0.39 (02)	−0.08 (02)	$17^- \rightarrow 15^-$	E2
470.7	3.1 (2)	0.40 (09)	−0.25 (12)	$13^- \rightarrow 11^-$	E2
476.2	82.1 (3)	0.34 (01)	−0.09 (01)	$10^+ \rightarrow 8^+$	E2
487.6 [a])	1.2 (1)			$6^- \rightarrow 5^+$	
488 [a])	1.0 (1)			$13^- \rightarrow (11^-)$	
492.5	5.6 (1)	0.35 (03)	−0.07 (03)	$13^- \rightarrow 11^-$	E2
497.6	79.0 (4)	0.31 (01)	−0.06 (01)	$12^+ \rightarrow 10^+$	E2
502 [a])	1.0 (5)			$13^- \rightarrow 11^-$	

TABLE 1—continued

E_γ [keV]	I_γ	A_2/A_0	A_4/A_0	Assignment	Assigned multipolarity
516.3 [b])	3.0 (3)			$15^- \rightarrow 13^-$	
522.3	69.3 (3)			$14^+ \rightarrow 12^+$	
523 [c])				$(14^-) \rightarrow 12^-$	
523.8 [c])				$14^- \rightarrow 12^-$	
529.4 [b])	2.0 (4)			$15^- \rightarrow 13^-$	
536.7	21.0 (1)	0.26 (01)	−0.08 (01)	$19^- \rightarrow 17^-$	E2
548.0 [a])	5.7 (4)			$15^- \rightarrow 13^-$	
554 [c])				$(16^-) \rightarrow (14^-)$	
555.3	50.4 (3)	0.34 (01)	−0.08 (01)	$16^+ \rightarrow 14^+$	E2
564.2	5.0 (2)	0.37 (07)	−0.10 (07)	$17^- \rightarrow 15^-$	E2
566.1 [a])	3.1 (3)			$16^- \rightarrow 14^-$	
569.8	4.7 (2)			$19^- \rightarrow 18^+$	
575 [d])				$(18^-) \rightarrow (16^-)$	
575.0 [d])	18.8 (2)	0.30 (02)	−0.09 (02)	$21^- \rightarrow 19^-$	E2
575.7 [d])				$18^{(+)} \rightarrow (16^+)$	
577.6 [a])	4.1 (3)			$17^- \rightarrow 15^-$	
586.8	34.4 (2)	0.31 (01)	−0.07 (01)	$18^+ \rightarrow 16^+$	E2
589.0 [c])				$18^- \rightarrow 16^-$	
601.3	14.3 (2)	0.29 (03)	−0.07 (03)	$23^- \rightarrow 21^-$	E2
603.4 [a])	1.7 (4)			$19^- \rightarrow 17^-$	
613.5				$8^- \rightarrow 8^+$	
613.6 [a])	3.6 (3)			$19^- \rightarrow 17^-$	
620.1 [a])	7.2 (3)			$17^- \rightarrow 16^+$	
624.6	22.2 (1)	0.31 (01)	−0.07 (01)	$20^+ \rightarrow 18^+$	E2
625.1 [a])	1.6 (2)			$(20^-) \rightarrow 18^-$	
643.7 [c])				$20^{(+)} \rightarrow 18^{(+)}$	
644.4	9.9 (1)	0.17 (03)	0.11 (02)	$25^- \rightarrow 23^-$	E2
653.8 [a])	1.2 (2)			$(21^-) \rightarrow 19^-$	
673.7	11.2 (1)	0.23 (02)	−0.08 (02)	$22^+ \rightarrow 20^+$	E2
682.8	1.2 (1)	0.37 (21)	−0.19 (20)	$21^- \rightarrow 19^-$	E2
686.7 [a])	1.2 (2)			$(22^-) \rightarrow (20^-)$	
695.1 [c])				$(22^+) \rightarrow 20^{(+)}$	
703.5	2.1 (1)	0.22 (11)	−0.14 (11)	$27^- \rightarrow 25^-$	E2
713.4	8.5 (1)	−0.25 (03)	0.02 (03)	$15^- \rightarrow 14^+$	E1
720.6 [a])	0.8 (1)			$(23^-) \rightarrow (21^-)$	
730.0	3.1 (1)	0.16 (06)	−0.04 (06)	$24^+ \rightarrow 22^+$	E2
770.5 [c])				$(29^-) \rightarrow 27^-$	
788.9 [b])	1.1 (2)			$(26^+) \rightarrow 24^+$	
798.9	1.4 (1)	0.40 (18)	−0.06 (16)	$4^+ \rightarrow 4^+$	E2/M1
843.7 [c])				$2^+ \rightarrow 0^+$	
849.4 [c])				$(28^+) \rightarrow (26^+)$	
870.5	1.4 (1)	0.25 (15)	0.32 (14)	$5^+ \rightarrow 4^+$	E2/M1
877.1	2.3 (1)	−0.08 (10)	0.13 (10)	$13^- \rightarrow 12^+$	E1
890.0 [c])				$13^- \rightarrow 12^+$	
1071.6	2.0 (1)	0.27 (10)	−0.08 (10)	$4^+ \rightarrow 2^+$	E2
1240.0 [b])	5.5 (7)			$5^- \rightarrow 4^+$	

[a]) Intensity is extracted from the total projection.
[b]) Intensity is extracted from gated spectra.
[c]) Unable to extract information on the transition.
[d]) The angular distribution and intensity of the 575.0 keV transition is really a summed contribution of the 575, 575.0 and 575.8 keV transitions.

first to establish the existence of a 1.1. ms isomer at 1843.8 keV. The radioactive decay studies of Finger *et al.* [8]) and Cailliau *et al.* [9]) established both a second 0^+ state at 492 keV, associated with the coexisting oblate structure, and a quasivibrational γ-band. In-beam studies by Burde *et al.* [10]) identified the yrast band up to the 16^+ level, while Beshai *et al.* [11]) extended the known levels of this band up to 20^+. The proposed level scheme for ^{184}Pt is shown in fig. 1. Four new transitions are added to the yrast band, and 6 new side bands labelled 2 through 7 are assigned. Two summed coincidence spectra are shown in fig. 2, corresponding to gates on bands 1 and 2. The cascade of band 1 is assigned up through the 948.4 keV transition, although angular distribution coefficients could not be extracted for the last two γ-rays. Band 2 becomes yrast at $I \approx 25$, which explains the slightly larger transition intensities in this band as compared to band 1 (yrast at lower spins). The parity of band 2 is established by the 345.3 keV transition between bands 2 and 5. The A_2/A_0 value of the 345.3 keV transition is positive, indicating either a stretched E2 or an $I \rightarrow I$ essentially pure dipole assignment. The former requires the same parity for

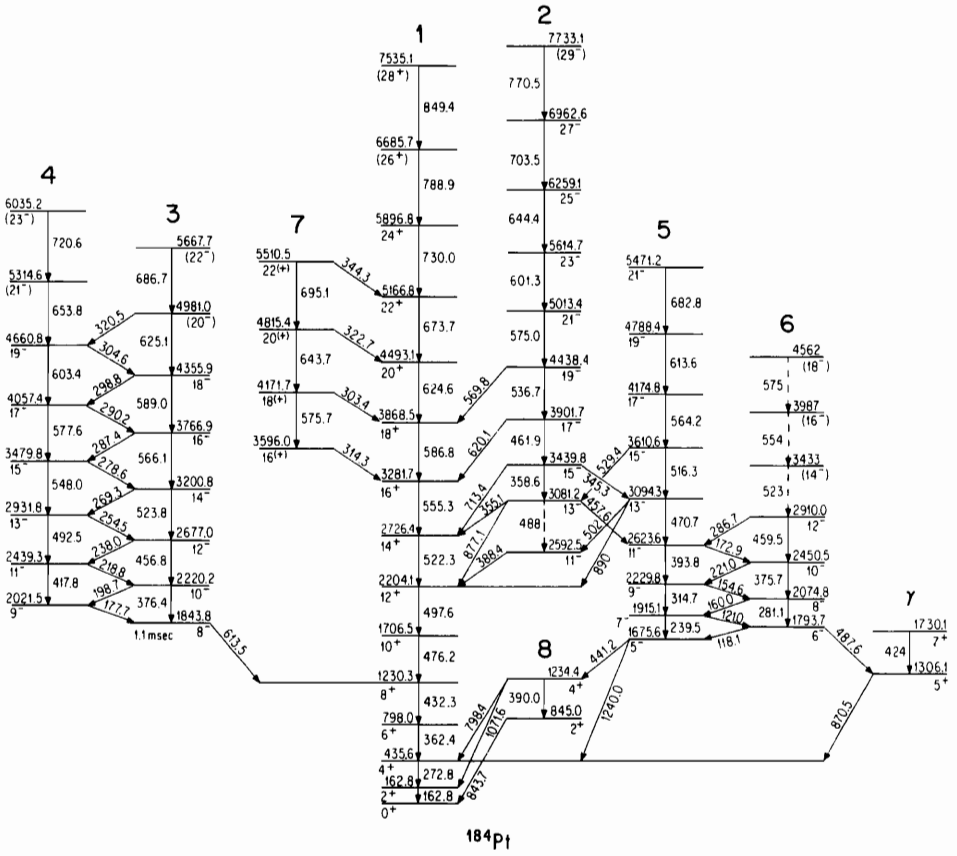

Fig. 1. Level structure of ^{184}Pt.

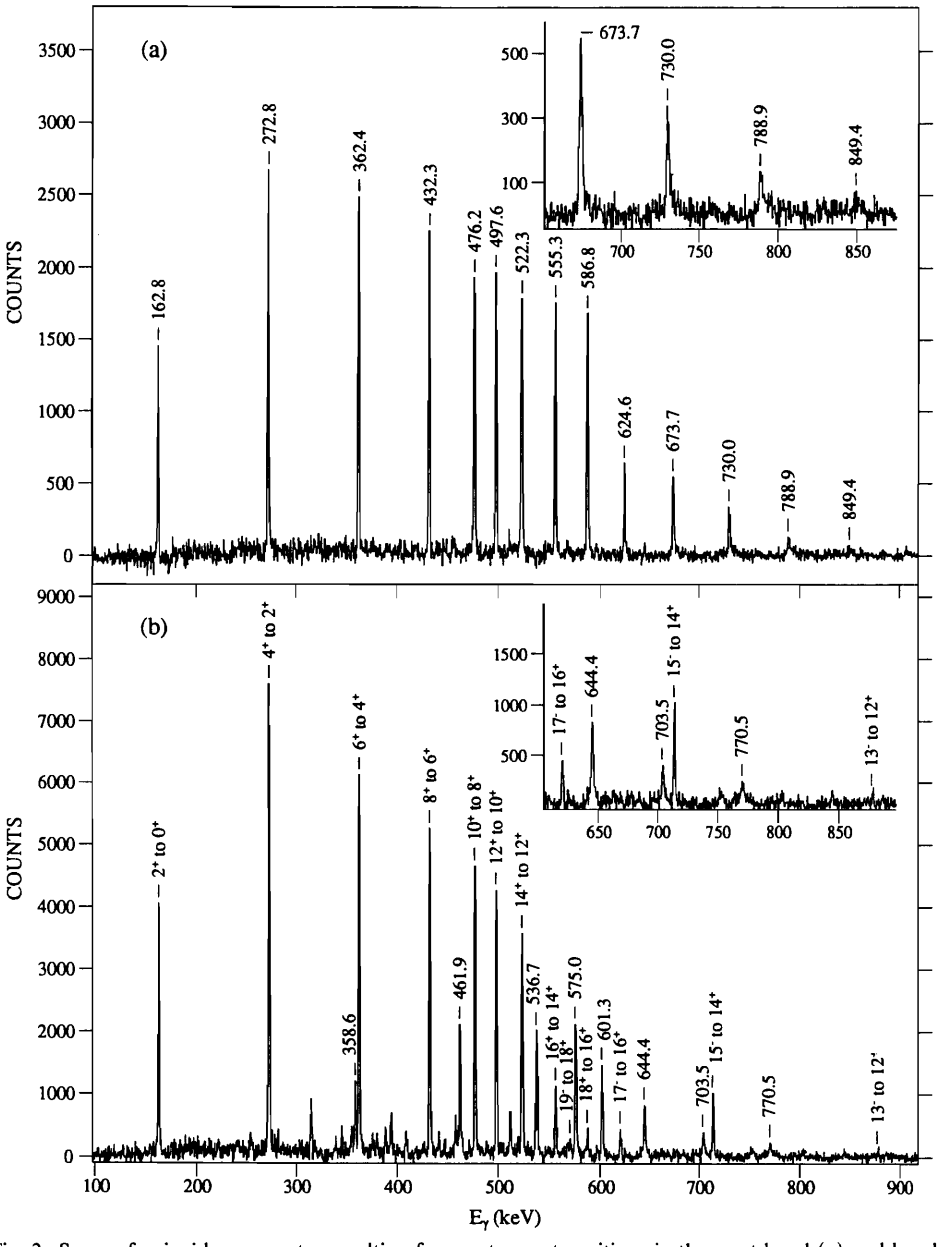

Fig. 2. Sums of coincidence spectra resulting from gates on transitions in the yrast band (a) and band 2 (b). For (a), the sharp drop-off in intensity of the last five transitions is partly due to the fact that gates on these transitions were used to create the summed spectrum. For (b), all E2 transitions in band 2 are labelled by their energy and are included in the sum of gates, while transitions associated with the yrast band and interband transitions connecting band 2 with the yrast band are labelled by the spin and parity of the initial and final state.

these two bands, and Burde *et al.* [7]) have measured the 1675.6 keV level as 5^- through a conversion electron experiment. The latter possibility could permit different parities for bands 2 and 5, but would require lowering the spins of band 2 by two units. This is impossible in view of the two transitions out of the 3081.2 keV level of band 2 to the 12^+ and 14^+ levels of the yrast band, establishing negative parity for band 2. The measured A_2/A_0 and A_4/A_0 coefficients of the 713.4 keV γ-ray indicate that it is a stretched dipole transition, leading to the assignment of odd spins to band 2.

Also Burde *et al.* [7]) established the 1793.7 keV level in band 6, but gave it an assignment of 6^+ based on the conversion coefficient of the 1181.1 keV transition. However, the large negative A_2 values of the 118.1 and 121.0 keV transitions suggest E2/M1 assignments, and thus negative parity also for band 6. The placements of the top three transitions (523, 554 and 575 keV) in band 6 are somewhat tentative, due to the apparent weak population of the corresponding levels and the presence of more intense γ-rays with similar energies, appearing elsewhere in the decay scheme. For example, a 523.8 keV transition in coincidence with a 577.6 keV transition is observed between bands 3 and 4, while both 575.0 and 575.7 keV transitions in bands 2 and 7, respectively, are in coincidence with the 555.3 and 522.3 keV transitions of the yrast band. One piece of evidence which lends strong support to the current assignments in band 6 is the gate on the 221.0 keV transition (10^- to 9^-), which clearly shows the three transitions in question. The fact that the gate does not show other members of the yrast band, which are not in coincidence with band 6, indicates that the background subtraction is reasonable. This is important, since the 554 and 523 keV transitions are also found in the yrast band, and one must be certain that their presence in a gate with poor statistics is not due to improper background subtraction.

Two strongly-coupled rotational bands labelled 3 and 4 in fig. 1 are thought to be built upon the 1843.8 keV (8^-) level. The spin, parity and lifetime of this state was first established by Burde *et al.* [7]). The 1.1 m lifetime is much longer than the time window for defining coincidence events (~100 ns) in our measurements, thus there are no coincidence data which link these two bands with any other band in ^{184}Pt. However, γ-rays in these bands have the same total energy and multiplicity distribution as known lines in ^{184}Pt, which leads to the placement of these two bands in ^{184}Pt. Such strongly coupled $K=8$ bands have been observed in the lower Z isotones of ^{184}Pt, e.g. ^{182}Os [ref. [12])]. Thus, the placement of these two bands on top of the 1843.8 keV level agrees well with the systematics of the even-even $N=106$ nuclei.

Band 7 decays to the yrast band via the 314.3, 303.4, 322.7, and 344.3 keV transitions. These are assigned as $\Delta I=0$ transitions based on the large positive A_2/A_0 values for the 303.4 and 322.7 keV lines, since the absence of large positive A_4/A_0 values rules out $\Delta I=1$ transitions. It is possible that these transitions could be assigned as $I \rightarrow I-2$, but then the levels of band 7 would be yrast which would disagree with the low population intensity in this band. We are unable to determine

the parity of the levels in this band, however a tentative assignment of positive parity has been given to them. This preferred assignment is based on the observation of a band in both ^{182}Pt [ref. [13])] and ^{180}Os [ref. [14])] which has been given the assignment ($\pi = +$, $\alpha = 0$)* and has an unusually strong feeding to the yrast band via $\Delta I = 0$ transitions. In these nuclei, weaker $\Delta I = 2$ transitions are also observed from these bands to the yrast band; however, in our data such transitions are not observed, presumably due to unfavorable branching ratios.

3. Band assignments

To investigate the nature of the observed bands and their crossings, we plot both the experimental aligned angular momentum (i) and quasiparticle routhian (e') as functions of rotational frequency (fig. 3). The former results from the subtraction of a reference angular momentum, $\omega(J_0+\omega^2 J_1)$, from the total angular momentum along the rotational axis, and the latter is calculated by subtracting a reference energy, $-\frac{1}{2}\omega^2 J_0 - \frac{1}{4}\omega^4 J_1 + \hbar^2/8J_0$, from the total excitation energy transformed into the rotating frame [15]). These reference parameters, J_0 and J_1, have been chosen to give a nearly constant alignment in the yrast band of ^{184}Pt after the band crossing.

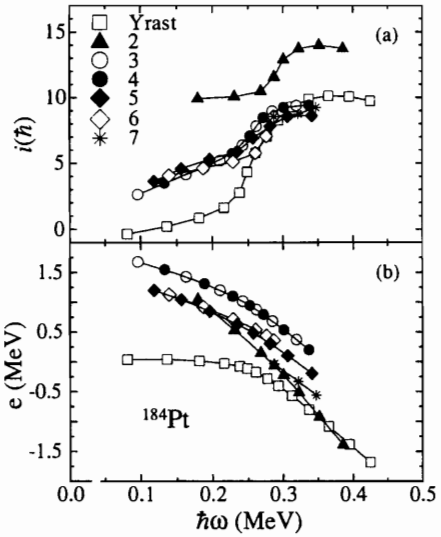

Fig. 3. Aligned angular momentum (a) and experimental routhians (b) as a function of rotational frequency for the observed bands in ^{184}Pt. The reference parameters ($J_0 = 22\hbar^2/\text{MeV}$, $J_1 = 110\hbar^4/\text{MeV}^3$) have been chosen to give an almost constant alignment in the yrast band of ^{184}Pt after the band crossing. K has been assumed to be zero for the yrast and for band 2, $K = 8$ for bands 3 and 4, and $K = 1$ for bands 5-7.

* The parity of the band is denoted by π, the signature by α. Band members have spins equal to α plus an even integer. For odd-A nuclei, $\alpha = \pm\frac{1}{2}$; for even-A, $\alpha = 0, 1$.

In order to make definite conclusions about the initial quasiparticle composition of the side bands in ^{184}Pt, we have extracted effective one-quasiparticle routhians and aligned angular momenta by averaging together the quasiparticle configurations observed in the adjacent odd-A nuclei. For the odd-N Pt nuclei, ^{183}Pt [ref. [16])] and ^{185}Pt [ref. [17])], these configurations have been associated with the asymptotic quantum numbers $[624]\frac{9}{2}^{+}(\nu i_{13/2})$, $[514]\frac{7}{2}^{-}$ $(\nu h_{9/2}+\nu f_{7/2})^{\star}$ and $[521]\frac{1}{2}^{-}$ $(\nu p_{3/2})^{\star\star}$. For the odd-$Z$ nuclei ^{185}Au [ref. [3])] and ^{183}Ir [ref. [18])] the observed quasiparticle states are $[541]\frac{1}{2}^{-}$ $(\pi h_{9/2})$, $[660]\frac{1}{2}^{+}$ $(\pi i_{13/2})$, $[530]\frac{1}{2}^{-}$ $(\pi f_{7/2})$, and $[402]\frac{5}{2}^{+}$ $(\pi d_{5/2})$. Table 2 contains the averaged experimental alignments and routhians for those configurations which are thought to make up the multi-quasiparticle bands in ^{184}Pt, using the reference parameters quoted above. These averaged routhian energies were extracted at $\hbar\omega = 0.175$ MeV, with the experimentally extracted pairing gaps, which are calculated using the prescription described in ref. [19]), having been added to them ($\Delta_p = 0.945$ and $\Delta_n = 1.068$ MeV). Also included in the table are the one-letter labels which are used in the text to relate these orbitals to the theoretically calculated routhians. The general convention for assigning letter labels to the theoretical quasiparticle routhians is summarized in table 3. Theoretical alignments (labelled CSM) were calculated from the cranked shell model, using deformation parameters ($\beta_2 = 0.225$, $\beta_4 = -0.03$, $\gamma = 0°$) extracted from the TRS calculations for the ground band in ^{184}Pt. It should be noted that even though the experimental routhian for

TABLE 2

Experimentally averaged (avg.) and theoretically calculated (CSM) alignments of the one-quasiparticle configurations which are thought to comprise the multi-quasiparticle bands in ^{184}Pt. Also included are the averaged quasiparticle energies extracted at $\hbar\omega = 0.175$ MeV

Nilsson level ($\hbar\omega = 0$)	(π, α)	Label	$i[\hbar]$		Avg. e' [MeV]
			avg.	CSM	
$[660]\frac{1}{2}^{+}$	$(+, +\frac{1}{2})$	a	6.8	6.5	0.995
$[541]\frac{1}{2}^{-}$	$(-, +\frac{1}{2})$	f	4.2	3.2	0.269
$[624]\frac{9}{2}^{+}$	$(+, +\frac{1}{2})$	A	4.0	4.0	0.629
$[624]\frac{9}{2}^{+}$	$(+, -\frac{1}{2})$	B	3.9	4.0	0.675
$[521]\frac{1}{2}^{-}$	$(-, +\frac{1}{2})$	H [a])	1.5	0.5	0.935
$[514]\frac{7}{2}^{-}$	$(-, +\frac{1}{2})$	F	2.2	1.0	1.037
$[514]\frac{7}{2}^{-}$	$(-, -\frac{1}{2})$	E	2.2	1.0	1.037

[a]) The $\nu p_{3/2}$ configuration is given a quasiparticle label (H) even though at low rotational frequency CSM calculations show that the second lowest lying negative-parity quasiparticle pair is strongly mixed with the third, fourth and fifth pairs (see cranked-shell-model diagrams presented in sect. 6.1).

* In ^{185}Pt, Pilotte *et al.* [17]) assign a $K = \frac{7}{2}$ band to be $[503]\frac{7}{2}^{-}$. The standard Nilsson scheme suggests $[514]\frac{7}{2}^{-}$ to be more likely for $N = 106$. Actually, this structure is a mixture of $f_{7/2}$ and $h_{9/2}$ components.

** The asymptotic quantum numbers assigned to these configurations are only valid in the absence of rotation. The labels in brackets refer to the spherical shell model state from which these levels originate.

TABLE 3

Convention for labeling the theoretical quasiparticle routhians of different parity and signature. Capital letters are used for neutron configurations, while lower case letters are used for proton configurations

Label	Parity (π)	Signature (α)
A, C, a, c	+	$+\frac{1}{2}$
B, D, b, d	+	$-\frac{1}{2}$
E, G, e, g	−	$-\frac{1}{2}$
F, H, f, h	−	$+\frac{1}{2}$

the $\nu p_{3/2}$ orbital lies lower than those for the two signatures of the ($\nu h_{9/2} + \nu f_{7/2}$) orbitals, we have chosen to label the $[514]\frac{7}{2}^+$ quasiparticles E and F. This is done to conform to the theoretical quasiparticle diagrams (presented in sect. 6.2), where the lowest lying negative-parity pair is associated with the E, F-orbitals with no signature splitting.

3.1. BAND 2

From fig. 3a, one can see that band 2 of ^{184}Pt has an initial alignment of $i = 10\hbar$. From the additivity of the experimental one-quasiparticle alignments listed in table 2, the only two-quasiparticle configuration which is able to give this much alignment for a negative-parity band is af, i.e. $\pi i_{13/2} \otimes \pi h_{9/2}$ (i_{sum} (exp) = 11.0$\hbar$ from table 2). Added support for this assignment comes from other indications:

(i) Band 2 becomes yrast at $\hbar\omega \approx 0.36$ MeV (see fig. 3b). The same phenomenon is observed in light Au nuclei (for example ^{185}Au, see ref. [3])) where the routhian for the $\pi i_{13/2}$ band initially lies high in energy and becomes yrast at $\hbar\omega \approx 0.3$ MeV. This similarity suggests that band 2 has an $\pi i_{13/2}$ component.

(ii) The absence of any signature partner for this band. Since both proposed quasiparticles have high j and low K, a doubly decoupled structure results with the unfavored signature lying significantly higher in energy than the favored signature.

(iii) The observation of a similar band in ^{182}Pt [ref. [13])], ^{185}Pt [ref. [17])] and ^{186}Pt [ref. [21])] but not in the even-even Os nuclei. This is due to the fact that the $\pi i_{13/2}$ $[660]\frac{1}{2}^+$ orbital lies too far above the Fermi level to be easily observed experimentally at $Z = 76$.

3.2. BANDS 3 AND 4

Bands 3-6, all of which have analogues in ^{182}Os, are assigned as two-quasineutron structures, and their alignments before the crossings are $i \approx 4$-$5\hbar$, which is approximately equal to the sum of the alignments of one $\nu i_{13/2}$ quasiparticle coupled with

either a $\nu h_{9/2}$ or $\nu p_{3/2}$ configuration in table 2. Bands 3 and 4, which are based on a 1.1 ms isomeric state, are most likely associated with the $[624]^{9+}_{\frac{9}{2}} \otimes [514]^{7-}_{\frac{7}{2}}$ neutron configuration as suggested by Burde *et al.* [7]), since these two orbitals are the only observed configurations in this region which reproduce the band-head spin ($I = 8$). The nature of the individual quasiparticles in the two-quasiparticle band is also determined by the lack of signature splitting observed between the bands (see fig. 3b). Table 4 tracks the energy difference between the two signatures of the $[624]^{9+}_{\frac{9}{2}}$ configuration as a function of N in both Pt and Os nuclei. In all cases, a measurable signature splitting is observed between the two components. On the other hand, little or no signature splitting is observed between the two components of the $[514]^{7-}_{\frac{7}{2}}$ configuration in the same odd-N Pt or Os nuclei. Therefore, we have concluded that bands 3 and 4 must couple the favored signature of the $[624]^{9+}_{\frac{9}{2}}$ (A) configuration with the two signatures of the $[514]^{7-}_{\frac{7}{2}}$ configuration (E and F), and thus we label bands 3 and 4 as AE and AF, respectively. The fact that no signature splitting is observed even at the highest spins, indicates that the E- and F-configurations must retain their high-K characteristics even under the condition of rotation.

3.3. BANDS 5 AND 6

We assign bands 5 and 6 to the $\nu i_{13/2} \otimes \nu p_{3/2}$ configuration. From fig. 3b, one can see that there is an observable energy splitting between the two bands. This signature splitting indicates that lower-K components are mixed into the wave functions for these bands. The magnitue of this splitting is comparable to that observed between the A- and B-signatures of the $i_{13/2}$ quasineutron bands of the odd-N nuclei listed in table 4. Thus, we conclude that bands 5 and 6 result from the coupling of the favored signature of the $\nu p_{3/2}$ $(-, +\frac{1}{2})$ quasiparticle with the two signatures of the $\nu i_{13/2}$ configuration, AH and BH.

3.4. BAND 7

From fig. 3a, band 7 has an alignment of 8-9$\hbar$. We have tentatively assigned positive parity to this band based on the fact that similar positive-parity bands with

TABLE 4

Experimental routhian energy differences (in MeV) between the two signatures of the $\nu i_{13/2}$ configuration A$(+, +\frac{1}{2})$ and B $(+, -\frac{1}{2})$ in Pt and Os nuclei taken at $\hbar\omega = 0.20$ MeV. This energy difference was extracted from the one-quasiparticle $i_{13/2}$ bands in the odd-N nuclei and from the lowest lying negative-parity bands in the even-even nuclei

N	102	103	104	105	106	107
Pt	0.102	0.079	0.095	0.082	0.031	0.031
Os		0.120	0.118	0.120	0.028	0.041

strong $\Delta I = 0$ interband transitions to the yrast band are observed in the neighboring even-even nuclei (see sect. 2.2). In ^{180}Os, it has been suggested that this band [labelled $(+,0)_4$ in ref. [14])] has the configuration $(\nu i_{13/2})^2$, even though the yrast structure is thought to have the same configuration in this frequency range. In ^{182}Os a low-lying positive-parity band is observed which has also been assigned the same configuration, and the level scheme suggests that it is a continuation of the γ-band [22]). Thus, the band in ^{180}Os may also be related to some type of vibrational structure as well, which would explain why one is able to observe a coexisting $(\nu i_{13/2})^2$ band. This structure may at the higher frequencies be composed of a mixture of the lowest 2 and 4 quasiparticle configurations within the $\nu i_{13/2}$ intruder shell. According to the quasiparticle diagrams presented in sect. 6.2, some of these excitations are predicted to have lower energies than the lowest negative-parity band. The configurations will, however, be strongly mixed due to the AB, BC, and AD crossings.

3.5. E2 TRANSITIONS BETWEEN BANDS 2 AND 5

One interesting feature in the level scheme is the observation of strong interband E2 transitions between the 15^- and 13^- states of bands 2 and 5. This is surprising since the two bands have very different structures, band 2 being two-quasiproton (af) in composition and band 5 being two-quasineutron (AH). However, the 13^- states in these bands lie only 13 keV apart and a certain configuration mixing can be expected which could explain the strong interband transitions. In order to estimate the configuration mixing of the two bands, we performed a two-level mixing calculation. The perturbed $I^\pi = 13^-$ states can be written in a form

$$|13^-, 3081\rangle = a|2\rangle + b|5\rangle\,,$$
$$|13^-, 3094\rangle = b|2\rangle - a|5\rangle\,, \qquad (1)$$

where $|2\rangle$ and $|5\rangle$ are the unperturbed wave functions of bands 2 and 5. With the assumption that the 15^- states are unmixed (they lie 171 keV apart), eq. (1) leads to the following B(E2) branching ratios for the 15^- to 13^- transitions:

$$\frac{B(\mathrm{E2}, 3440 \to 3094)}{B(\mathrm{E2}, 3440 \to 3081)} = \frac{b^2}{a^2}\,,$$
$$\frac{B(\mathrm{E2}, 3611 \to 3081)}{B(\mathrm{E2}, 3611 \to 3094)} = \frac{b^2}{a^2}\,. \qquad (2)$$

Measured branching ratios yield values of 0.52 ± 0.17 and 0.53 ± 0.08 for these two respective B(E2) ratios. The good agreement between the two values verifies the assumption of just a two-level mixing. Using the average value $b^2/a^2 = 0.52$, one obtains $a = 0.81$ and $b = 0.59$ for the wave function amplitudes, with an interaction

matrix element of only 6.3 keV. Considering the structural differences between the two bands, it is not surprising that the interaction between them is so small.

4. Band crossings in ^{184}Pt and neighboring nuclei

Perhaps the key question to be answered concerning the physics of the high-spin states observed in ^{184}Pt and its neighbors is the nature of the first yrast-band crossing. While it is clear that the rotational alignment of a pair of $i_{13/2}$ quasineutrons is responsible for the first yrast crossing in the deformed nuclei for $N = 90$ and higher, the question is still very much debated for $N \approx 106$ nuclei. Already in 1978, Kahler *et al.* [20]) suggested from a measurement of bands in ^{185}Au that the first band crossing occurred due to the alignment of $h_{9/2}$ quasiprotons. This question had been considered earlier by Beshai *et al.* [11]) through their measurement of the band crossing in ^{184}Pt. More recently, Larabee *et al.* [3]) proposed that both $\nu i_{13/2}$ and $\pi h_{9/2}$ alignments are taking place below $\hbar\omega = 0.30$ MeV in ^{185}Au and ^{184}Pt. Janzen *et al.* [18]) concluded that a low-frequency $\pi h_{9/2}$ crossing is present in the $\nu i_{13/2}$ band of ^{185}Pt from an analysis of $B(M1)/B(E2)$ ratios. Also, Hebbinghaus *et al.* [21]) have suggested that the pattern of band crossings in ^{186}Pt is best explained by a low-frequency $\pi h_{9/2}$ alignment process. On the other hand, it is quite difficult to theoretically produce a $\pi h_{9/2}$ crossing so low in frequency, in spite of the fact that this orbital ($[541]\frac{1}{2}^-$) is the ground state of odd-A Au and Ir nuclei with $N \leqslant 108$. Schiffer and Garrett [23]) have also discounted a $\pi h_{9/2}$ crossing below $\hbar\omega = 0.3$ MeV, based upon an analysis of band crossings due to high-j *low-K* states. Assuming a reasonable value of the proton pairing gap and the maximum alignment achievable, they concluded that the $h_{9/2}$ band crossing should be around $\hbar\omega = 0.4$ MeV.

A number of new measurements have been performed not only on $N = 106$ nuclei (e.g. ^{184}Pt described herein), but also on $N = 107$ and 108 isotones. The alignment systematics of the bands of interest in $N = 106$, 107 and 108 isotopes of Ir, Pt and Au are gathered in fig. 4. It is important to discuss fully the arguments for and against the proposed $\pi h_{9/2}$ alignment process as an explanation for some of the many band crossings seen in fig. 4. It is clear that the alignment of high-j quasiprotons will have an important role in the formation of any largely- or super-deformed shape in this region. Thus, we must understand where the alignment of the first of these, namely $\pi h_{9/2}$, actually occurs.

In the $N = 106$ and $N = 107$ nuclei, most experimentally observed rotational bands in the elements Os, Ir, Pt and Au give evidence for at least one band crossing in the frequency interval $0.20 < \hbar\omega < 0.35$ MeV. The observed band crossings (fig. 4) seem to follow the following rules:

(i) In bands with an excited $i_{13/2}$ neutron a single band crossing is observed, associated with a spin alignment of about $5\hbar$.

(ii) In bands with an excited $h_{9/2}$ proton a single band crossing with an alignment of about $5\hbar$ is also observed.

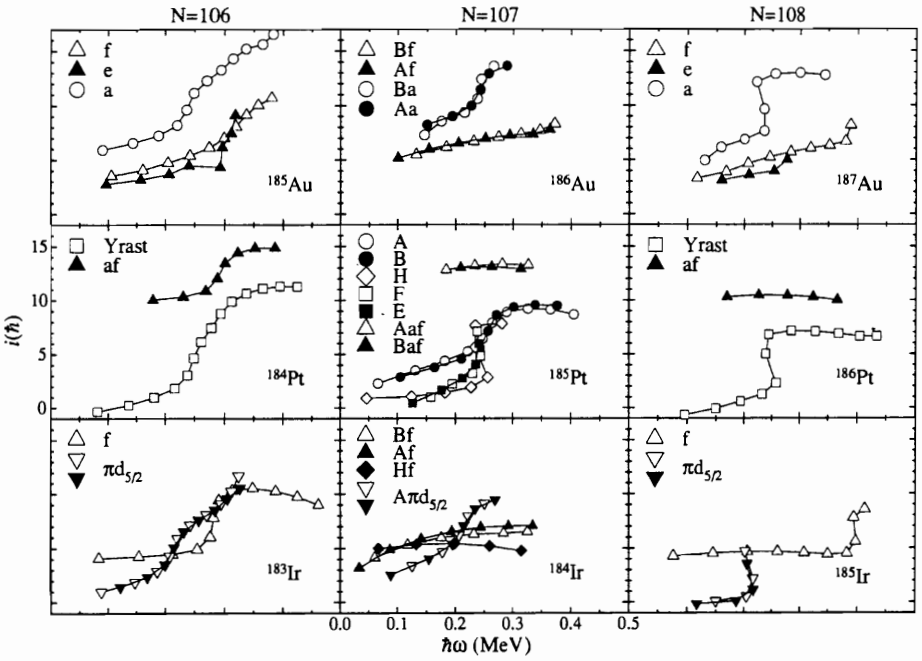

Fig. 4. Alignment diagrams for the bands of interest in the region of ^{184}Pt. A common reference has been used for all bands ($J_0 = 22\hbar^2/\text{MeV}$, $J_1 = 90\hbar^4/\text{MeV}^3$). The ^{184}Pt results are from the present work, while the results for the other cases come from the literature: ^{183}Ir, ref. [18]); ^{185}Au, ref. [3]); ^{184}Ir, ref. [27]); ^{185}Pt, ref. [18]); ^{186}Au, ref. [26]); ^{185}Ir, ref. [25]); ^{186}Pt, ref. [21]); ^{187}Au, ref. [24]).

(iii) In bands with both an excited $i_{13/2}$ neutron and an excited $h_{9/2}$ proton no band crossing is observed below $\hbar\omega = 0.35$ MeV.

(iv) In bands without excited $i_{13/2}$ neutrons or $h_{9/2}$ protons at least one but in certain configurations two distinguishable band crossings are observed below $\hbar\omega \approx 0.35$ MeV. Independent of whether it is possible to distinguish two band crossings or not, the aligned angular momentum, i, approaches $10\hbar$ in those bands that have been followed to sufficiently high frequencies, suggesting that two band crossings (which sometimes may have nearly degenerate frequencies) appear in these bands.

The observed band crossings can be explained in a rather consistent way using two very different approaches. *In the first approach* (described in sect. 5) it is assumed that all the bands have similar deformations and that therefore standard blocking arguments can be used. This leads to an interpretation in which the alignment of $h_{9/2}$ protons plays a crucial role at frequencies below 0.35 MeV.

In the second approach (described in sect. 6) the deformation of each band is determined from cranking calculations using the Woods-Saxon potential. Since all band crossings are deformation dependent, a given band crossing may appear at very different frequencies depending on the deformation of the considered configuration and normal blocking arguments cannot be used. In this approach nearly all

low-lying band crossings are explained as alignments of $i_{13/2}$ neutrons, the $h_{9/2}$ protons being involved only in exceptional cases.

In the $N = 108$ isotones the band crossing pattern is slightly different due to the large gap in the single-particle energy spectrum at this neutron number. Nevertheless both of the above-mentioned approaches allow for a consistent interpretation of the band crossings observed at $N = 108$ also.

5. Experimental information on band crossings

In the following, the band crossings are discussed in terms of the quasiparticle notation defined in table 3. The first neutron crossing is then AB ($\nu i_{13/2}$) and the first proton crossing ef ($\pi h_{9/2}$). If the AB crossing is blocked by a quasiparticle in the A(B) level, then the secondary BC (AD) crossing is expected at a somewhat higher frequency than the AB crossing. In the same way, the scondary $\pi h_{9/2}$ crossing can be labelled eh or fg. Furthermore, in a band for which the AB crossing is not blocked, a second $\nu i_{13/2}$ crossing (CD) will appear after the AB alignment has occurred, perhaps at a frequency within our detection limit. If experimentally observed rotational bands have similar deformations, blocking arguments can be used to determine the character of the aligning quasiparticles, as described in the remainder of sect. 5. The resulting assignments for the nature of the many band crossings in this region are listed in table 5, and are discussed in the following sections. Alternative quasiparticle assignments for the band crossings come from the theoretical analysis of sect. 6, and are also listed in table 5.

5.1. EVIDENCE FOR $\pi h_{9/2}$ CROSSINGS AT $N = 108$

Fig. 4 shows the alignment systematics of the bands of interest for the Ir, Pt and Au nuclei at $N = 106$, 107 and 108. Starting our analysis at $N = 108$, the figure shows that the yrast band in ^{186}Pt experiences a sharp band crossing at $\hbar\omega \approx 0.25$ MeV with an alignment gain (Δi) of approximately $7\hbar$. The $\pi i_{13/2} \otimes \pi h_{9/2}$ (af) two-quasiparticle band in ^{186}Pt indicates no crossing up to $\hbar\omega = 0.37$ MeV. As discussed by Hebbinghaus *et al.* [21]), this pattern suggests that the observed alignment in the yrast band is due to $h_{9/2}$ quasiprotons, since this crossing is blocked in the two-quasiproton sideband. This analysis also implies that the $(\nu i_{13/2})^2$ (AB) band crossing must be delayed beyond $\hbar\omega = 0.37$ MeV. Support for this interpretation comes from the adjacent odd-Z nuclei as well. In ^{187}Au [ref. [24])], the $\pi i_{13/2}$ band experiences a band crossing at $\hbar\omega \approx 0.23$ MeV with $\Delta i \approx 6\hbar$, while the $\pi h_{9/2}$ band exhibits no crossings before $\hbar\omega = 0.39$ MeV. In ^{185}Ir [ref. [25])], the $\pi h_{9/2}$ band exhibits a first crossing at $\hbar\omega \approx 0.40$ MeV, while for the $\pi d_{5/2}$ band, where the $\pi h_{9/2}$ crossing is not blocked, the beginning of an alignment occurs at $\hbar\omega \approx 0.21$ MeV.

Therefore, the blocking analysis leads to the conclusion that there is a $\pi h_{9/2}$ crossing at $\hbar\omega \leq 0.25$ MeV in these observed bands at $N = 108$: the yrast band of ^{186}Pt, the $\pi d_{5/2}$ band of ^{185}Ir, and the $\pi i_{13/2}$ band of ^{187}Au (see table 5). The crossing

TABLE 5

Observed crossings in bands in the region illustrated in fig. 4.

Nucleus	Band	Observed $\hbar\omega_c$ (MeV)	Blocking scenario	Theoretical scenario		
			aligning pair [b]	aligning pair	approx. γ before (after) [c] crossing	comment
(a) $N = 106$						
^{183}Ir	f	0.28	AB	AB	0° (−5°)	ef blocked
	$\pi d_{5/2}$	0.21, 0.30	AB, ef	AB, CD	−15°	ef high
^{184}Pt	g	0.26, 0.30	AB, ef	AB, CD	−5° (−15°)	ef high
	AE, AF, AH, BH	0.26	ef	BC (AD)	−15° (−20°)	ef high
	af	0.29	AB	AB	10°	ef blocked
^{185}Au	f, e	0.32	AB	AB	5° (−10°)	ef blocked
	a	0.24, 0.30	AB, ef	AB, ef	10° (15°)	Δ_p reduced
(b) $N = 107$						
^{184}Ir	$A\pi d_{5/2}$	0.21	ef	BC	−20°	ef high
^{185}Pt	A, B	0.25	ef	BC (AD)	−15°	ef high
	E, F, H	0.25	AB or ef [d]	AB, CD [d]	−10°	ef high
^{186}Au	Aa, Ba	0.24	ef	ef	10°	Δ_p reduced
(c) $N = 108$						
^{185}Ir	f	0.40	eh or AB	AB	0°	ef blocked
	$\pi d_{5/2}$	0.21	ef	AB	−15° (−20°)	ef high
^{186}Pt	g	0.25	ef	AB	−10° (−30°)	ef high
^{187}Au	f	0.39	eh or AB	AB	5°	ef blocked
	a	0.23	ef	ef	10°	Δ_p reduced

Two possibilities for the aligning quasiparticles are given, one from the analysis of the experimental data using a blocking scenario (sect. 5 in the text) and the other from a theoretical analysis utilizing predicted shape changes. The γ-values are rounded off to an accuracy of 5°.

[a]) In the bands Af, Bf (in ^{184}Ir and ^{186}Au), Aaf, Baf (in ^{185}Pt) and af (in ^{186}Pt) no band crossing is observed, and is not expected to appear below $\hbar\omega \approx 0.35$ MeV in either of the two scenarios. These bands are therefore not included in the table.

[b]) In cases where two quasiparticle pairs align, the order is not known or suggested.

[c]) The γ-value after the crossing is given in parenthesis if it deviates more than 5° from the value before the crossing.

[d]) Only the first of the two expected crossings has so far been observed.

frequencies for the latter two of these is less than that in ^{186}Pt possibly because of partial pairing blocking, i.e. a slight reduction of the proton pairing due to the blocking of one orbital by the valence proton.

A further indication that the AB quasineutron crossing moves up significantly in rotational frequency at $N = 108$ comes from an examination of the yrast bands in the even-even W nuclei. In fig. 5 is shown the angular momentum along the rotation axis, I_x, as a function of rotational frequency for the yrast bands in W, Os and Pt nuclei. The first band crossing in W-nuclei occurs systematically between $\hbar\omega = 0.2$ and 0.3 MeV for $N = 96$ to 106. But from the figure it is clear that there is a large

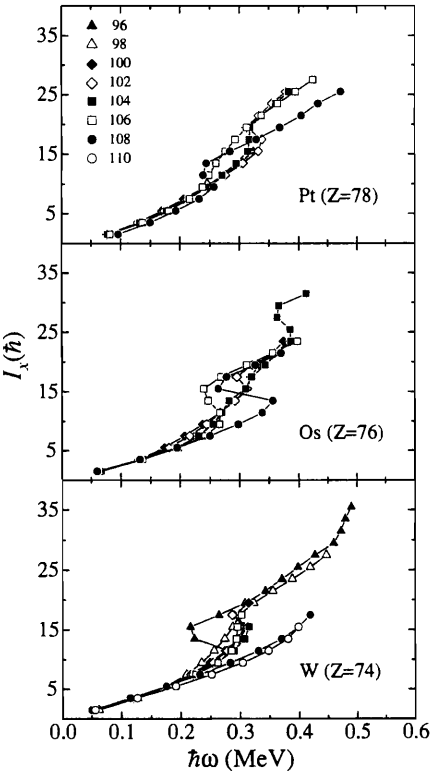

Fig. 5. Diagram of the angular momentum projected onto the rotational axis, I_x, versus the rotational frequency, $\hbar\omega$, for W, Os an Pt isotopes. The ^{184}Pt results come from the present work, while the results for the other cases come from the literature: ^{170}W, ref. [29]); ^{172}W, ref. [30]); ^{174,176}W, ref. [31]); ^{178}W, ref. [32]); ^{180,182,184}W, ref. [33]); ^{176,178}Os, ref. [34]); ^{180}Os, ref. [14]); ^{182}Os, ref. [12]); ^{184}Os, ref. [35]); ^{176,178}Pt, ref. [36]), ^{180}Pt, ref. [37]); ^{182}Pt, ref. [13]); ^{186}Pt, ref. [21]).

jump in the frequency at which the $(\nu i_{13/2})^2$ band crossing occurs in the $N = 108$ W isotope. The sudden disappearance of the AB neutron crossing probably arises from a gap in the single-particle levels at $N = 108$. This gap moves the Fermi surface further away from the low-K orbitals, which leads to a large increase in the crossing frequency.

5.2. EVIDENCE FOR $\pi h_{9/2}$ CROSSINGS AT $N = 107$

At $N = 107$, there is also evidence that $h_{9/2}$ quasiprotons align at frequencies below $\hbar\omega = 0.30$ MeV. Fig. 4 shows that in the odd-odd nucleus ^{186}Au [ref. [26])] a single crossing at $\hbar\omega \approx 0.24$ MeV is observed in bands with the configuration $\nu i_{13/2} \otimes \pi i_{13/2}$ (Aa and Ba), while no crossing is observed in bands with the configuration $\nu i_{13/2} \otimes \pi h_{9/2}$ (Af and Bf). Since the $\nu i_{13/2}$ band crossing is blocked in both cases and the $\pi h_{9/2}$ crossing is blocked only for the Af and Bf bands, the single band crossing observed in the Aa and Ba bands is most likely due to $h_{9/2}$ quasiprotons

as opposed to secondary neutron crossings BC or AD. Data on ^{184}Ir [ref. [27])] also give evidence that the neutron crossings have moved up infrequency at $N = 107$. That is, bands with the configuration $\nu i_{13/2} \otimes \pi h_{9/2}$ (Af and Bf) and $\nu p_{3/2} \otimes \pi h_{9/2}$ (Hf) experience no crossings below $\hbar\omega = 0.32$ MeV. The latter is especially important, because it indicates that $\hbar\omega_c$ (AB) is above 0.32 MeV in this band, while the former two only put constraints on the BC and AD crossings. Furthermore, the bands which do not block the $\pi h_{9/2}$ crossing, namely the two signatures of $\nu i_{13/2} \otimes \pi d_{5/2}$ in fig. 4, experience a band crossing at $\hbar\omega \approx 0.21$ MeV. From blocking arguments, the conclusions for the nature of this alignment is the same as that for the Aa and Ba bands in ^{186}Au: it is due to $\pi h_{9/2}$ quasiparticles.

In ^{185}Pt [ref. [17])], all one-quasiparticle bands experience a crossing at around $\hbar\omega \approx 0.25$ MeV, while the three-quasiparticle band $\nu i_{13/2} \otimes \pi i_{13/2} \otimes \pi h_{9/2}$ (Aaf and Baf) does not. One might propose therefore, that all one-quasiparticle bands in ^{185}Pt experience the $h_{9/2}$ quasiproton alignment. Janzen *et al.* [18]) have measured the $B(M1)/B(E2)$ ratios in the $\nu i_{13/2}$ band in ^{185}Pt and have found a significant rise in these ratios after the upbend. They go on to show that theoretical calculations in the framework of existing models can only explain this increase if the aligning quasiparticles are a pair of protons, assuming that the $B(E2)$ values behave as expected. However, in order to be conclusive, the $B(E2)$ values have to be measured separately, and the theoretical models improved to properly describe multi-quasiparticle configurations in triaxially deformed nuclei.

The conclusion from a blocking analysis of $N = 107$ nuclei is that the alignment of $\pi h_{9/2}$ (ef) quasiparticles is responsible for the crossings in the $A\pi d_{5/2}$ bands of ^{184}Ir, in bands A and B (and possibly E, F, and H) of ^{185}Pt, and in the Aa and Ba bands of ^{186}Au (see table 5).

5.3. $N = 106$: EVIDENCE FOR A $\pi h_{9/2}$ CROSSING

At $N = 106$, the $\nu i_{13/2}$ band crossing (AB) occurs at $\hbar\omega \approx 0.28$ and 0.26 MeV in ^{180}W [ref. [33])] and ^{182}Os [ref. [12])], respectively. Based on these systematics and the above discussion on the Pt nuclei at $N = 107$ and 108, it then seems to be a reasonable proposal that both $\nu i_{13/2}$ and $\pi h_{9/2}$ quasiparticles are aligning at nearly degenerate frequencies in ^{184}Pt, as proposed by Larabee *et al.* [3]).

From the alignment plot for ^{184}Pt in fig. 3a, the yrast band exhibits an upbend with an alignment gain of approximately $11\hbar$, while sidebands 2-6 experience upbends with a Δi of $5\text{-}6\hbar$. In band 2, whose quasiparticle configuration is $\pi h_{9/2} \otimes \pi i_{13/2}$, the observed band crossing at $\hbar\omega \approx 0.29$ MeV must be due to $i_{13/2}$ (AB) quasineutrons since the $\pi h_{9/2}$ band crossing is blocked. As discussed above, the $\nu i_{13/2}$ band of ^{185}Pt appears to experience a $\pi h_{9/2}$ alignment at $\hbar\omega \approx 0.25$ MeV with a $\Delta i \approx 5\hbar$. The sum of the Δi values in ^{185}Pt and band 2 is close to the alignment in the yrast band after its crossing, which suggests the possibility that both proton and neutron band crossings are present in the yrast sequence of ^{184}Pt [ref. [4])]. It

seems reasonable to assign the $\hbar\omega \approx 0.26$ MeV crossings in the two-neutron sidebands also to the $\pi h_{9/2}$ alignment, since this frequency is similar to that of ^{185}Pt.

In ^{183}Ir [ref. [18])] and ^{185}Au [ref. [3])], similar alignment differences are observed between bands with and without a $\pi h_{9/2}$ composition. In ^{183}Ir, rotational bands built on the $\pi h_{9/2}$ and $\pi d_{5/2}$ ($[402]^{5+}_{\frac{5}{2}}$) orbitals are observed, and it is clear from fig. 4 that the alignment gains for these two bands are quite different. In the $\pi h_{9/2}$ band, a crossing of $\Delta i \approx 6\hbar$ is observed at $\hbar\omega \approx 0.28$ MeV. For the $\pi d_{5/2}$ bands, Δi is at least $10\hbar$ and the interaction region occurs over a frequency range comparable to that for the yrast band in ^{184}Pt. The conclusions are also similar: two crossings occur in both ^{184}Pt and ^{183}Ir. The $\pi h_{9/2}$ band undergoes the expected $\nu i_{13/2}$ crossing, while the $\pi d_{5/2}$ band experiences both the neutron and proton crossings. Furthermore, Janzen *et al.* [18]) have measured $B(M1)/B(E2)$ values in the $\pi d_{5/2}$ band of ^{183}Ir and found a small decrease through the first crossing. This is compatible with the assignment of this crossing as based on proton rather than neutron alignment.

For ^{185}Au, rotational bands built on the $\pi i_{13/2}$ ($[660]^{1+}_{\frac{1}{2}}$) and $\pi h_{9/2}$ configurations are observed [3]). The crossing region in the $\pi i_{13/2}$ band parallels quite closely the yrast band in ^{184}Pt and gains roughly the same amount of alignment. By comparison, the crossing in the $\pi h_{9/2}$ band of ^{185}Au has Δi of only $6.5\hbar$ and a crossing frequency delayed to $\hbar\omega \approx 0.32$ MeV, indicating that the extra alignment in the $\pi i_{13/2}$ band is also due to two band crossings.

It is, therefore, feasible to propose $\pi h_{9/2}$ crossings in the $\pi d_{5/2}$ band of ^{183}Ir, the yrast and two-neutron bands of ^{184}Pt, and the $\pi i_{13/2}$ band of ^{184}Au. One difficulty with this scenario is that the I_x values for the yrast bands in ^{184}Pt is similar to the I_x gain in the Os and W yrast bands after the first band crossing (see fig. 5), suggesting that the same alignment process is responsible for the first band crossing in all of these nuclei. Since the Os and W alignments have been attributed solely to $\nu i_{13/2}$ band alignments, this calls into some question the conclusions in this section and in sect. 5.1 that there are both neutron and proton crossings in the yrast band of ^{184}Pt.

6. Theoretical calculations concerning shape parameters and band crossings

In order to investigate the influence of shape effects on the rotational properties of nuclei in the Pt–Au transitional region, we have performed deformation self-consistent Strutinsky–Bogolyubov cranking calculations using a non-axial Woods–Saxon potential and parameters described in ref. [38]). Average pairing effects are included as the BCS pairing for the vacuum state at $\hbar\omega = 0$ MeV (Δ_0) coupled with a phenomenological approximation for the pairing gap at non-zero rotational frequencies. This approximation takes the form

$$\Delta(\omega) = \begin{cases} \Delta_0[1 - \frac{1}{2}(\omega/\omega_c)^2] & \omega \leqslant \omega_c, \\ \frac{1}{2}\Delta_0(\omega_c/\omega)^2 & \omega > \omega_c, \end{cases} \tag{3}$$

where $\omega_c = 0.40$ for even-N, 0.50 for odd-N, 0.50 for even-Z and 0.60 for odd-Z. If the particle number for either N or Z were odd, Δ_0 was renormalized to 87.5% of its initial value to simulate pair-blocking brought about by the odd particle. The frequency dependence of Δ is such that it on the average is close to the one obtained in calculations with particle-number projection. The deformation space covers $\beta_2 \cos(\gamma + 30°)$ from 0.05 to 0.40, $\beta_2 \sin(\gamma + 30°)$ from -0.20 to 0.30 and β_4 from -0.08 to 0.04 in steps of 0.04 around β_4 values favored by the liquid-drop energy, while the rotational frequency varies from 0.0 to 0.6 MeV. A detailed description of these calculations will be published in a separate paper [5]).

The total routhian of a nucleus (Z, N) of fixed many-quasiparticle configuration ν is given by:

$$E'(\hat{\beta}, N, Z, \nu) = E_{\mathrm{Str}}(\hat{\beta}, N, Z, \nu, \omega = 0) + \{\langle \Psi^{\omega} | H^{\omega} | \Psi^{\omega} \rangle_{\hat{\beta}, N, Z, \nu} - \langle \Psi^{\omega} | H^{\omega} | \Psi^{\omega} \rangle^{\omega=0}_{\hat{\beta}, N, Z, \nu}\} . \quad (4)$$

The first term on the right-hand side of eq. (4) represents the Strutinsky energy at $\hbar\omega = 0$ MeV while the second term represents the energy gain due to collective rotation and single-particle alignment. For the construction of total routhian surfaces (TRS), this energy is minimized with respect to the deformation parameter β_4.

6.1. DEFORMATION PARAMETERS FOR VARIOUS QUASIPARTICLE EXCITATIONS IN ^{184}Pt

Selected examples of total routhian surfaces for different quasiparticle configurations are given in fig. 6. Extracted equilibrium deformations plotted in the (β_2, γ) plane for the vacuum and lowest lying two- and four-quasiparticle excitations in ^{184}Pt are shown in fig. 7. Information associated with each plotted equilibrium deformation is listed in table 6. We have only included what we consider to be pure quasiparticle configurations. Frequencies close to a band crossing, where a pair of quasiparticles are only partially aligned, have therefore been excluded. The frequency interval is in most cases the one in which the considered configuration is closest to the yrast line. However, if a configuration is very mixed in this interval, because of near-lying band-crossings, we have included frequencies (usually lower ones) at which the configuration is pure but further away from the yrast line. At "prolate" shape we have included all configurations which possibly could be identified with any of the observed bands. For most of these configuration coexisting minima appear at "oblate" shape. These minima have also been included in fig. 7 and table 6. It should be observed that at "oblate shape" the proton levels labelled e and f originate from the $h_{11/2}$ subshell and not from the $h_{9/2}$ subshell as is the case for "prolate" shape.

Table 6 has been made quite detailed in order to allow the reader to draw his own conclusions about the likelihood of the two scenarios for the interpretation of

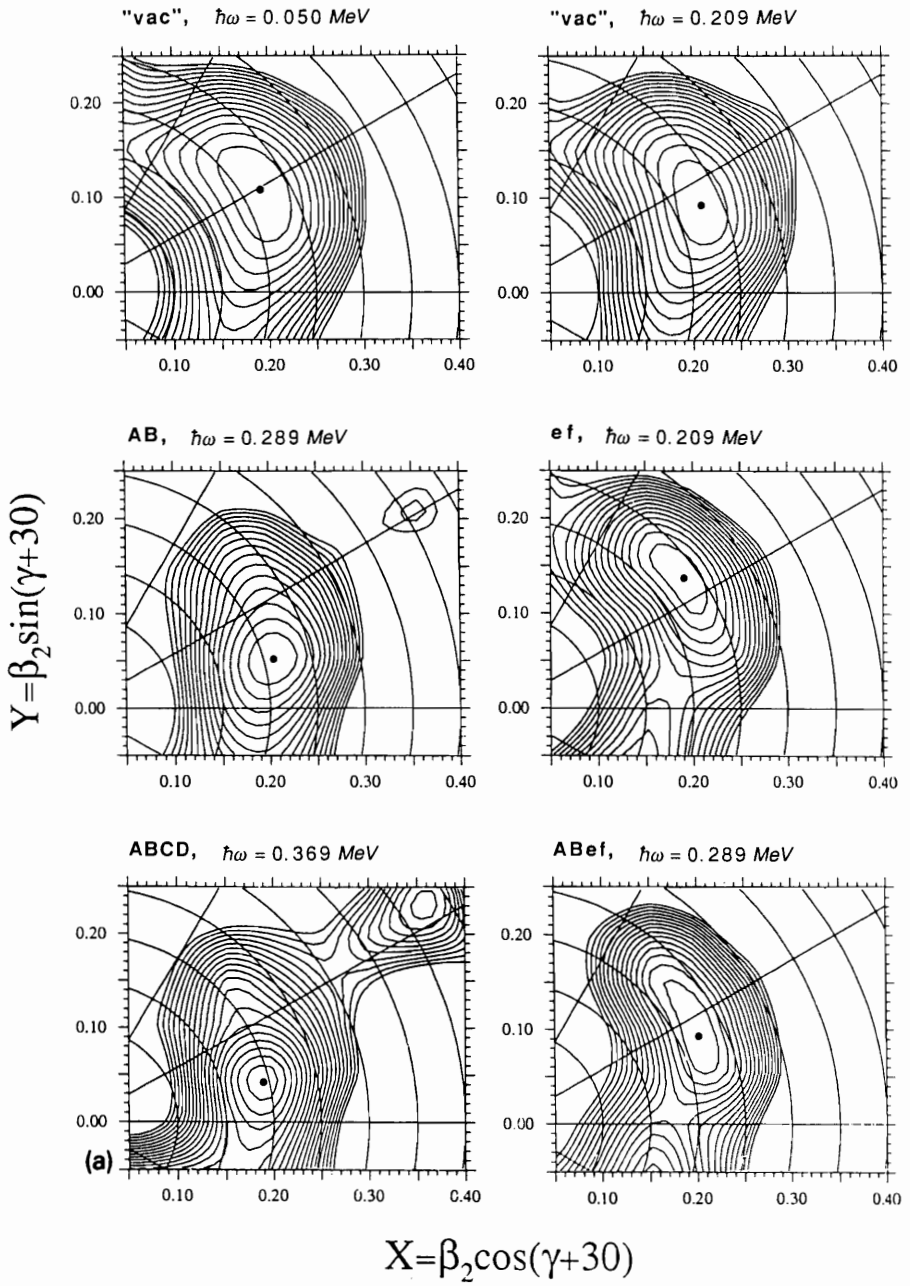

Fig. 6a. Example of TRS plots for those configurations in ^{184}Pt which are possible candidates for being yrast in certain frequency intervals. The selected frequencies do not always lie in these intervals, as we want to show pure configurations (see the first part of sect. 6.1). The indicated configurations refer to the minimum point (marked ●). Higher-lying minima, which appear in some of the plots, have a different configuration. The separation between contour lines is 0.1 MeV. Spin and energy in the minima are given in table 6.

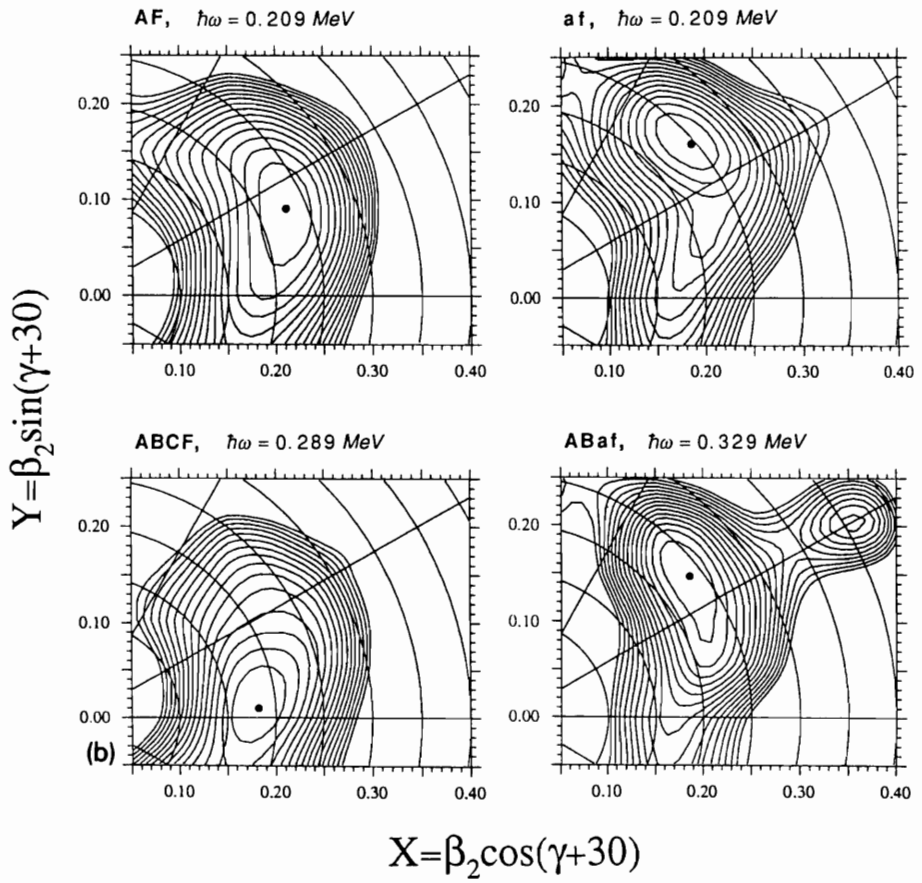

Fig. 6b. Examples of TRS-plots for some negative-parity configurations in ^{184}Pt. For details see caption to fig. 6a.

the band crossings. It must however be emphasized that the pairing has not been treated self-consistently. The pairing gap actually used (eq. (3)) may in certain configurations deviate significantly from the optimal value. *Since energies and spins depend quite sensitively on the pairing correlations, the values given in table* 6 *should not be used for direct quantitative comparisons with experimental data, but rather should be taken as a qualitative guideline.* The deformations, however, are much less sensitive to the pairing correlations, which can be seen by comparing fig. 7 with the corresponding figure in ref. [40]). The deformations in ref. [40]) were calculated assuming a quite different frequency dependence for Δ, where Δ decreased much faster with increasing frequency (approximately as in calculations without particle number projection).

6.1.1. Yrast band. The evolution of shape of the yrast band as a function of rotational frequency is shown in fig. 7a. The ground configuration is labelled as "vac" in the figure. At low frequencies, the prolate ground band corresponds to a

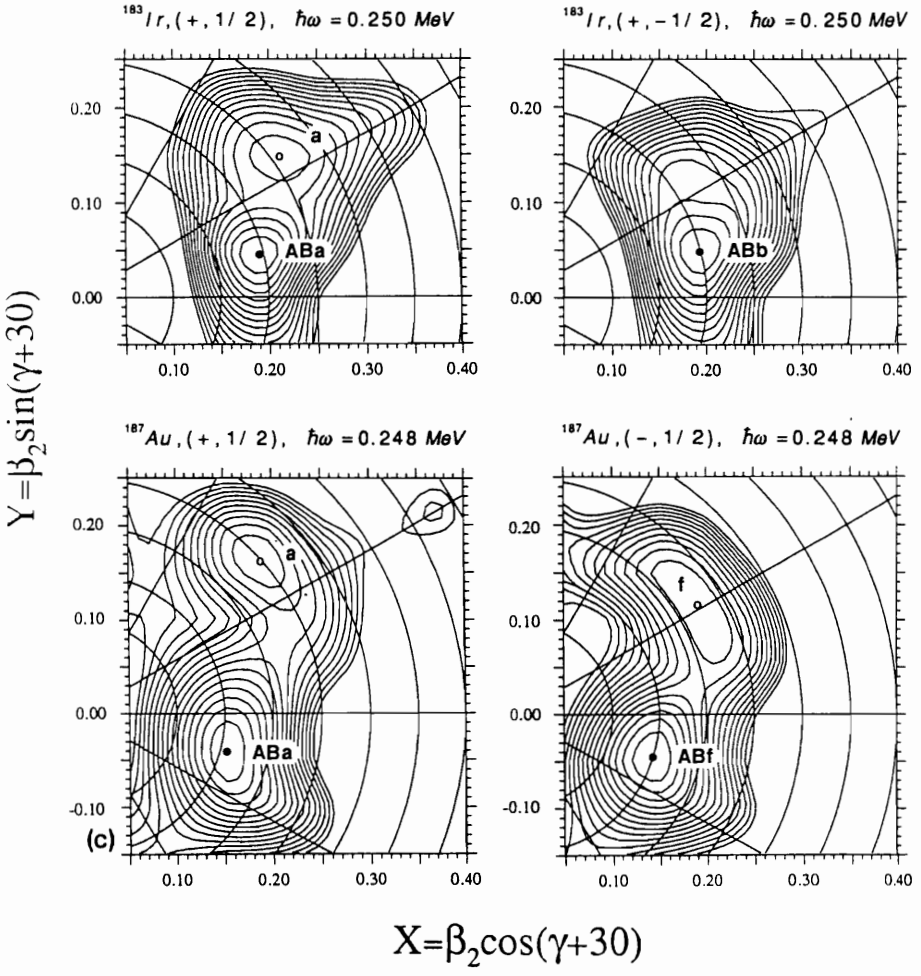

Fig. 6c. Selected TRS-plots for configurations in odd-proton ^{183}Ir and ^{187}Au. These surfaces show several examples of shape coexistence. Note that in the $(+,\frac{1}{2})$ surfaces a is a $\pi i_{13/2}$ particle in the minimum at $\gamma > 0°$ but an $N = 4$ particle in the minimum at $\gamma < 0°$. In the $(+,-\frac{1}{2})$ surface b is an $N = 4$ particle. In this case there is no coexisting minimum at $\gamma > 0°$ corresponding to a configuration b ($i_{13/2}$). This is a result of the large signature splitting between the lowest (a and b) $i_{13/2}$ quasiproton routhians, which disfavors the b-configuration energetically. In the $(-,\frac{1}{2})$ surface f is an $h_{9/2}$ particle at $\gamma \approx 0°$, whereas for $\gamma < -30°$ it is an $h_{11/2}$ particle. A and B are in all cases $i_{13/2}$ neutrons. The separation between contour lines is the same as in fig. 6a.

shape with quadrupole deformation gradually increasing from $\beta_2 = 0.219$ to 0.229 due to the centrifugal stretching. This prolate ground band "coexists" with an excited oblate ground band which is also shown in fig. 7a. Lifetimes for the yrast levels have been measured by Garg *et al.*[41]) up to $I^\pi = 16^+$. They observe an increase in $B(E2)$ values up to $I = 10\hbar$, which has been explained both by the mixing of the prolate ground band with the excited oblate band (the mixing decreases with

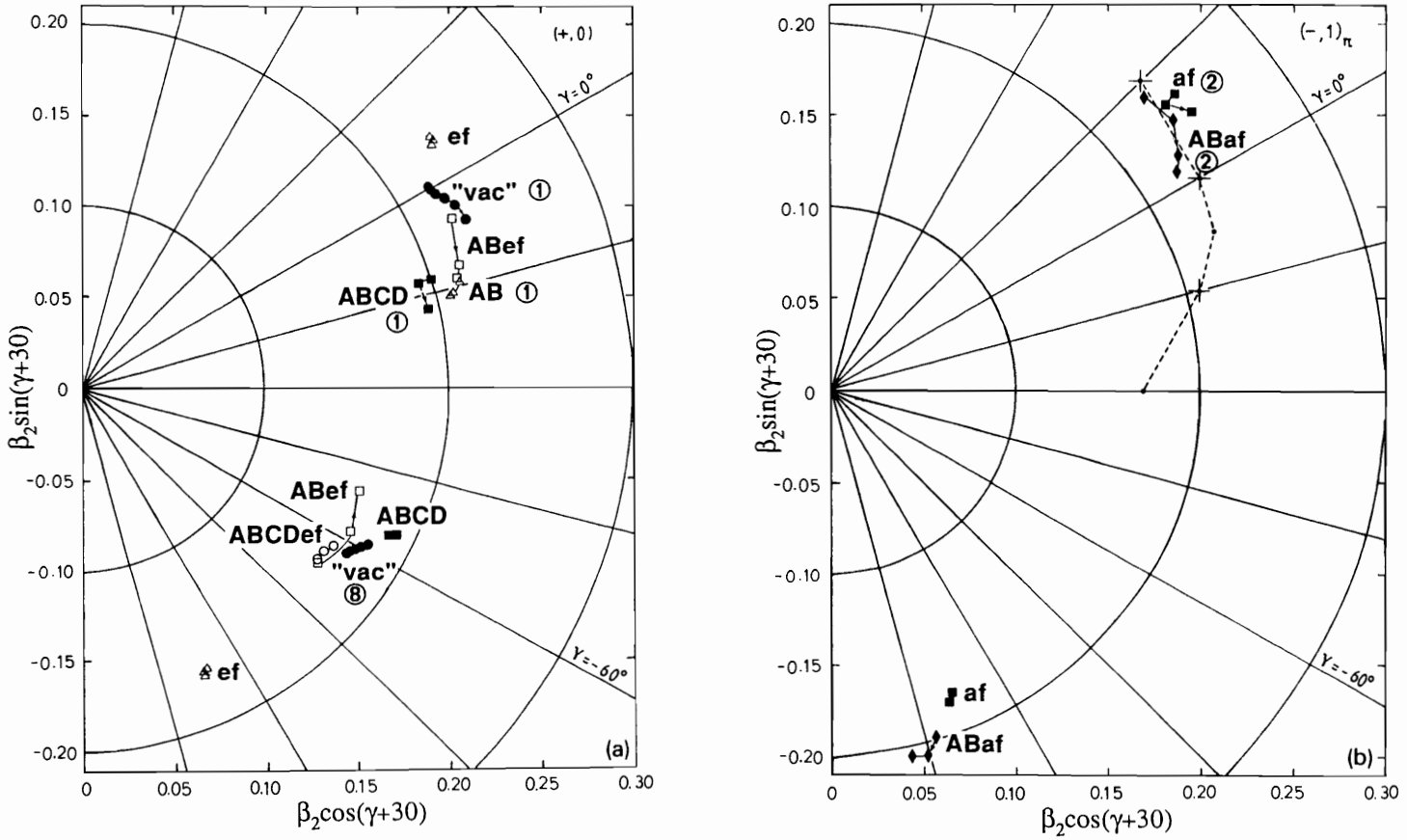

Fig. 7a, b. Calculated equilibrium deformations (β_2, γ) for several low-lying quasiparticle configurations in ^{184}Pt. The routhians were minimized at each (β_2, γ) grid point with respect to the hexadecapole deformation β_4, before the energy was minimized in the (β_2, γ) plane. For each configuration several deformations, corresponding to different rotational frequencies, are included. They are connected with lines and the arrows show the direction of increasing rotational frequency. The configuration labels used are those defined in table 3. The numbers used to identify the experimental bands (see fig. 1) are also shown encircled for some of the configurations. Additional information about each deformation, including β_4, proton and neutron spin, and the total routhian energy, can be found in table 6. For easy identification, the x ($=\beta_2\cos(\gamma+30°)$) and y ($=\beta_2\sin(\gamma+30°)$) coordinates are included in table 6. Notice that the proton levels e and f originate from the $h_{9/2}$ subshell for prolate shapes, $\gamma \geq -30°$, but from the $h_{11/2}$ shell for oblate shapes. The dashed line in (b) shows the trajectory along which the crossing frequencies in fig. 9 are calculated. The quasiparticle diagrams shown in fig. 8 are calculated at deformations along the line marked +.

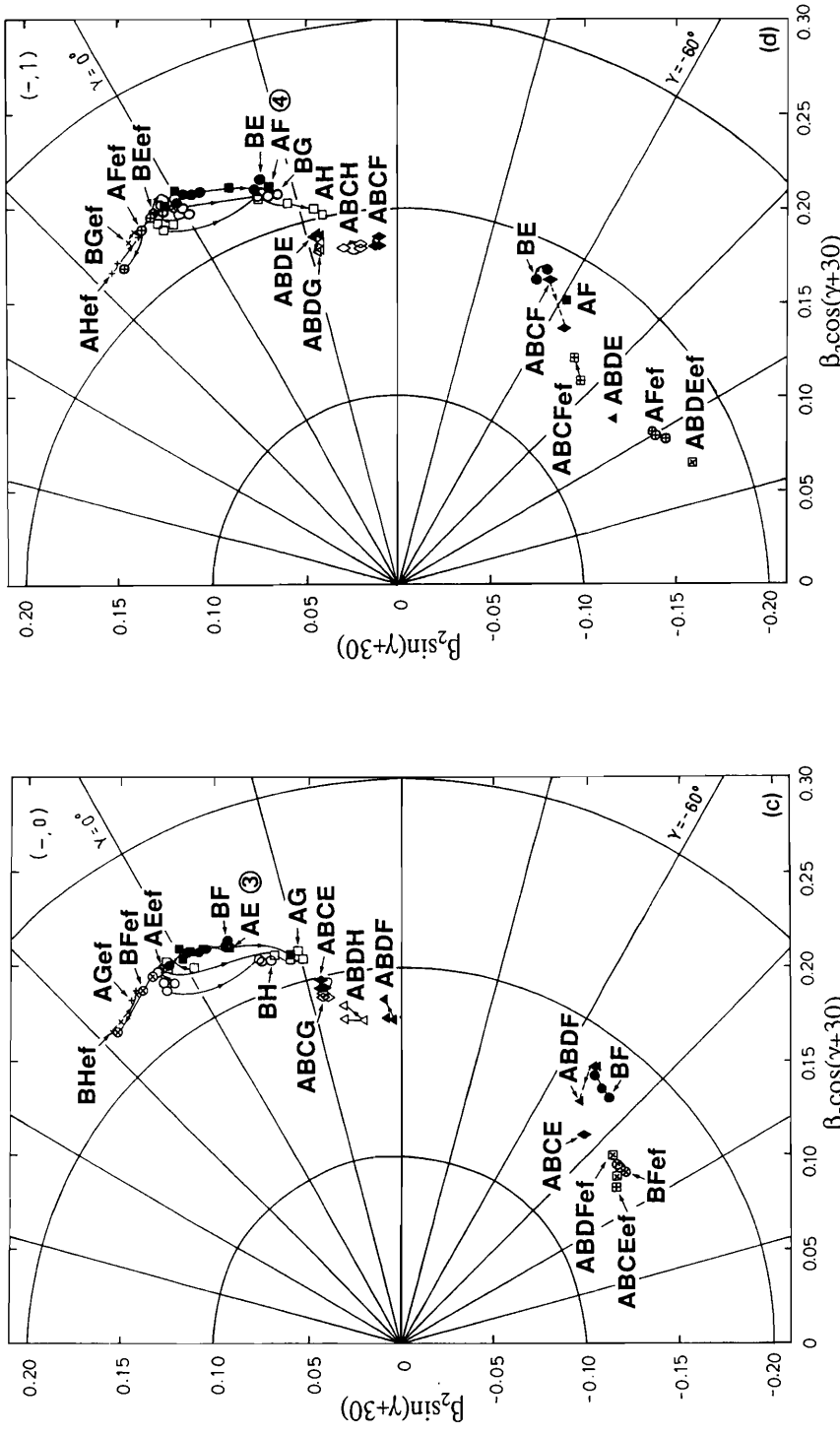

Fig. 7c, d. Same as fig. 7a, b but for the (−, 0) and (−, 1) configurations.

TABLE 6

Calculated equilibrium deformations (β_2, β_4, γ) for the observed and predicted bands in ^{184}Pt as functions of rotational frequency, $\hbar\omega$. Values for the proton (I_{xZ}) and the neutron (I_{xN}) contributions to the projection of the angular momentum on the rotational axis are also tabulated, as well as the total routhian energy, E' (given relative to the spherical liquid drop energy at $\hbar\omega = 0$). The $x(=\beta_2 \cos(\gamma+30°))$ and $y(=\beta_2 \sin(\gamma+30°))$ coordinates used in fig. 7, showing the equilibrium deformations, are also included. The configuration labels are the ones defined in table 3. The notation "prolate" is used for bands with $\gamma \geq -30°$ and "oblate" for bands with $\gamma < -30°$. *The information given in this table should not be used before carefully having read the first two paragraphs of sect. 6.1.*

$\hbar\omega$ [MeV]	β_2	γ	β_4	I_{xZ} [$\hbar$]	I_{xN} [$\hbar$]	E' [MeV]	x	y
Configuration: prolate vac (+, 0)								
0.000	0.219	0.09	−0.030	0.00	0.00	−2.828	0.190	0.110
0.050	0.220	−0.43	−0.030	0.29	0.84	−2.844	0.192	0.109
0.090	0.222	−1.30	−0.030	0.54	1.59	−2.907	0.194	0.106
0.130	0.224	−2.43	−0.030	0.84	2.47	−3.014	0.199	0.104
0.169	0.227	−3.75	−0.030	1.19	3.65	−3.172	0.204	0.100
0.209	0.229	−6.19	−0.030	1.63	5.79	−3.413	0.210	0.092
Configuration: prolate AB (+, 0)								
0.249	0.214	−14.16	−0.038	1.94	13.73	−3.919	0.206	0.058
0.289	0.210	−15.69	−0.040	2.34	16.40	−4.664	0.203	0.052
0.329	0.208	−16.14	−0.042	2.88	18.36	−5.516	0.202	0.050
Configuration: prolate ABCD (+, 0)								
0.130	0.199	−12.78	−0.043	0.80	17.47	−0.337	0.190	0.059
0.169	0.192	−12.80	−0.044	1.04	18.98	−1.197	0.184	0.057
0.369	0.194	−17.07	−0.045	3.25	23.04	−6.318	0.189	0.043
Configuration: prolate ef (+, 0)								
0.130	0.233	5.17	−0.032	6.49	2.37	−1.340	0.191	0.134
0.169	0.234	5.95	−0.033	6.99	3.36	−1.772	0.190	0.138
0.209	0.235	5.71	−0.034	7.35	4.85	−2.282	0.191	0.137
Configuration: prolate ABef (+, 0)								
0.289	0.222	−5.22	−0.041	7.86	14.86	−3.830	0.202	0.093
0.329	0.217	−12.11	−0.044	8.39	17.93	−4.936	0.206	0.067
0.369	0.213	−13.54	−0.047	8.15	20.59	−6.152	0.205	0 060
Configuration: oblate vac (+, 0)								
0.000	0.170	−61.86	−0.004	0.00	0.00	−2.264	0.145	−0.090
0.050	0.172	−61.28	−0.004	0.16	0.39	−2.241	0.147	−0.089
0.090	0.173	−60.61	−0.003	0.30	0.74	−2.271	0.149	−0.088
0.130	0.175	−59.70	−0.003	0.45	1.18	−2.318	0.152	−0.087
0.169	0.178	−58.66	−0.002	0.63	1.76	−2.381	0.156	−0.086
Configuration: oblate ABCD (+, 0)								
0.130	0.188	−55.18	0.008	0.53	19.30	−0.209	0.170	−0.080
0.169	0.185	−55.64	0.008	0.69	20.01	−0.716	0.167	−0.080
Configuration: oblate ef (+, 0)								
0.130	0.175	−97.03	−0.022	9.62	0.15	−1.454	0.066	−0.156
0.169	0.169	−96.71	−0.022	9.86	0.21	−1.866	0.067	−0.155
0.209	0.172	−97.39	−0.022	10.26	0.22	−2.285	0.066	−0.158
Configuration: oblate ABef (+, 0)								
0 209	0.160	−66.74	−0.011	9.59	12.16	−1.935	0.128	−0.095
0.249	0.165	−58.07	−0.006	9.27	13.62	−2.847	0.146	−0.078
0.289	0.161	−50.47	−0.004	8.42	15.26	−3.763	0.151	−0.056
Configuration: oblate ABCDef (+, 0)								
0.130	0.161	−62.18	−0.005	9.19	19.58	1.612	0.137	−0.086
0.169	0.159	−64.00	−0.004	9.53	20.34	0.281	0.132	−0.089
0.209	0.159	−66.29	−0.003	9.83	20.38	−1.097	0.128	−0.094

TABLE 6—continued

$\hbar\omega$ [MeV]	β_2	γ	β_4	I_{xZ} [$\hbar$]	I_{xN} [$\hbar$]	E' [MeV]	x	y
Configuration: prolate af $(-,1)_\pi$								
0.209	0.246	10.78	−0.026	11.26	4.70	−2.141	0.186	0.161
0.289	0.240	10.52	−0.031	11.72	7.11	−3.548	0.182	0.156
0.329	0.249	7.85	−0.030	12.14	8.73	−4.457	0.196	0.152
Configuration: prolate ABaf $(-,1)_\pi$								
0.289	0.233	13.24	−0.028	11.72	11.37	−3.845	0.170	0.160
0.329	0.237	8.31	−0.029	12.13	14.14	−4.864	0.186	0.147
0.369	0.228	4.07	−0.032	12.95	17.39	−6.060	0.189	0.128
0.409	0.223	2.33	−0.036	13.21	20.57	−7.385	0.188	0.119
Configuration: oblate af $(-,1)_\pi$								
0.130	0.177	−98.17	−0.024	3.83	0.14	−0.745	0.066	−0.165
0.169	0.178	−98.05	−0.024	4.63	0.20	−0.941	0.066	−0.165
0.209	0.182	−98.91	−0.024	5.13	0.26	−1.155	0.065	−0.170
Configuration: oblate ABaf $(-,1)_\pi$								
0.169	0.199	−103.38	−0.026	5.12	8.22	−0.329	0.057	−0.190
0.209	0.196	−102.91	−0.026	5.43	8.62	−0.972	0.058	−0.188
0.249	0.207	−105.28	−0.025	5.91	8.57	−1.590	0.053	−0.200
0.289	0.205	−107.37	−0.020	5.89	9.12	−2.145	0.045	−0.200
Configuration: prolate AE$(-,0)$								
0.000	0.236	−0.18	−0.031	0.00	1.88	−1.079	0.204	0.117
0.050	0.241	−0.32	−0.030	0.34	2.69	−1.287	0.209	0.119
0.090	0.239	−0.77	−0.030	0.62	4.48	−1.473	0.208	0.117
0.130	0.237	−1.61	−0.030	0.91	6.02	−1.745	0.208	0.113
0.169	0.234	−3.10	−0.031	1.24	7.56	−2.094	0.209	0.106
0.209	0.230	−6.27	−0.032	1.63	9.36	−2.516	0.210	0.092
0.249	0.215	−13.89	−0.039	1.95	11.79	−3.096	0.206	0.060
Configuration: prolate ABCE $(-,0)$								
0.289	0.198	−17.07	−0.044	2.17	21.11	−3.924	0.193	0.044
0.329	0.193	−17.59	−0.045	2.59	22.16	−5.029	0.189	0.042
0.369	0.193	−17.26	−0.046	3.23	23.83	−6.189	0.189	0.043
Configuration: prolate AEef $(-,0)$								
0.209	0.237	3.30	−0.035	7.28	8.58	−1.374	0.198	0.130
0.249	0.236	2.70	−0.037	7.62	9.94	−2.127	0.199	0.128
Configuration: prolate BF $(-,0)$								
0.000	0.237	1.85	−0.031	0.00	1.86	−1.076	0.201	0.125
0.050	0.241	−0.27	−0.030	0.34	2.71	−1.288	0.209	0.119
0.090	0.239	−0.63	−0.030	0.62	4.44	−1.472	0.208	0.117
0.130	0.236	−1.31	−0.030	0.91	6.00	−1.743	0.207	0.114
0.169	0.234	−2.35	−0.030	1.23	7.43	−2.090	0.208	0.109
0.209	0.233	−3.45	−0.030	1.62	8.79	−2.503	0.209	0.104
0.249	0.232	−6.22	−0.030	2.13	10.30	−2.969	0.212	0.094
0.289	0.234	−6.55	−0.030	2.83	11.70	−3.550	0.215	0.093
Configuration: prolate ABDF $(-,0)$								
0.289	0.173	−27.35	−0.032	2.08	20.43	−3.471	0.173	0.008
0.329	0.172	−28.51	−0.033	2.53	22.13	−4.556	0.172	0.004
0.369	0.183	−27.19	−0.037	3.26	23.80	−5.705	0.183	0.009
Configuration: prolate BFef $(-,0)$								
0.209	0.236	4.15	−0.035	7.30	8.47	−1.377	0.195	0.133
0.249	0.233	6.15	−0.035	7.67	9.65	−2.139	0.188	0.138
0.289	0.225	12.37	−0.038	8.08	10.19	−3.019	0.166	0.152

TABLE 6—continued

$\hbar\omega$ [MeV]	β_2	γ	β_4	I_{xZ} [$\hbar$]	I_{xN} [$\hbar$]	E' [MeV]	x	y
Configuration: prolate AG (−, 0)								
0.000	0.227	−0.88	−0.030	0.00	2.07	−0.877	0.199	0.111
0.050	0.238	1.93	−0.030	0.32	2.68	−1.019	0.202	0.126
0.090	0.235	2.10	−0.030	0.57	4.46	−1.200	0.199	0.125
0.130	0.217	−11.51	−0.032	0.89	7.25	−1.500	0.206	0.069
0.169	0.213	−13.64	−0.034	1.19	8.81	−1.900	0.204	0.060
0.209	0.212	−15.10	−0.034	1.53	10.45	−2.372	0.204	0.054
0.249	0.216	−14.78	−0.035	1.98	11.80	−2.939	0.208	0.057
Configuration: prolate ABCG (−, 0)								
0.289	0.190	−17.34	−0 040	2.07	21.26	−3.756	0.186	0.042
0.329	0.188	−17.69	−0.042	2.50	22.08	−4.866	0.184	0.040
0.369	0.189	−17.41	−0.042	3.13	23.65	−6.035	0.184	0.041
Configuration: prolate AGef (−, 0)								
0.169	0.234	7.23	−0.033	7.08	6.91	−0.424	0.187	0.142
0.209	0.232	8.48	−0.034	7.52	7.99	−1.100	0.182	0.145
Configuration: prolate BH (−, 0)								
0.000	0.227	2.23	−0.030	0.00	2.31	−0.899	0.192	0.121
0.050	0.235	2.95	−0.030	0.31	2.83	−1.022	0.197	0.128
0.090	0.230	3.51	−0.030	0.53	4.54	−1.207	0.192	0.127
0.130	0.226	3.60	−0.030	0.76	5.99	−1.472	0.188	0.125
0.169	0.219	−9.63	−0.031	1.20	7.85	−1.819	0.205	0.076
0.209	0.218	−9.84	−0.032	1.54	9.05	−2.223	0.204	0.075
0.249	0.216	−11.16	−0.033	1.94	10.04	−2.751	0.204	0.070
Configuration: prolate ABDH (−, 0)								
0.289	0.175	−20.07	−0.037	1.98	17.93	−3.314	0.173	0.030
0.329	0.173	−23.44	−0.037	2.38	21.01	−4.348	0.172	0.020
0.369	0.182	−20.27	−0.041	3.01	22.50	−5.446	0.180	0.031
Configuration: prolate BHef (−, 0)								
0.209	0.226	12.65	−0.033	7.77	8.42	−1.183	0.166	0.153
0.249	0.228	11.23	−0.034	7.98	9.56	−1.966	0.171	0.150
0.289	0.233	7.50	−0.038	7.82	10.46	−2.887	0.185	0.142
Configuration: oblate ABCE (−, 0)								
0.289	0.148	−71.36	−0.006	1.90	20.70	−3.522	0.111	−0.098
Configuration: oblate ABCEef (−, 0)								
0.289	0.143	−84.39	−0.011	11.03	18.83	−3.560	0.083	−0.116
Configuration: oblate BF (−, 0)								
0.130	0.173	−70.66	−0.006	0.36	9.38	−1.065	0.131	−0.112
0.169	0.174	−68.47	−0.005	0.50	10.01	−1.525	0.136	−0.108
0.209	0.177	−65.91	−0.003	0.72	10.68	−2.007	0.143	−0.104
Configuration: oblate ABDF (−, 0)								
0.169	0.180	−65.17	0.003	0.56	18.51	−0.543	0.147	−0.104
0.209	0.180	−65.62	0.003	0.71	20.00	−1.461	0.147	−0.105
0.329	0.161	−66.74	−0.003	1.11	21.58	−4.909	0.129	−0.096
Configuration: oblate BFef (−, 0)								
0.130	0.152	−82.87	−0.017	9.95	9.08	−0.141	0.092	−0.121
0.169	0.151	−81.62	−0.017	9.93	9.58	−1.002	0.094	−0.118
0.209	0.151	−80.79	−0.015	9.57	10.00	−1.883	0.095	−0.117
Configuration: oblate ABDFef (−, 0)								
0.289	0.146	−82.58	−0.011	10.87	18.72	−3.800	0.089	−0.116
0.329	0.152	−78.85	−0.009	10.56	19.84	−5.101	0.100	−0.114

TABLE 6—continued

$\hbar\omega$ [MeV]	β_2	γ	β_4	I_{xZ} [$\hbar$]	I_{xN} [$\hbar$]	E' [MeV]	x	y
Configuration: prolate AF (−, 1)								
0.000	0.237	1.85	−0.031	0.00	1.84	−1.075	0.201	0.125
0.050	0.241	−0.32	−0.030	0.34	2.70	−1.288	0.209	0.119
0.090	0.239	−0.71	−0.030	0.62	4.41	−1.471	0.208	0.117
0.130	0.236	−1.56	−0.030	0.91	5.99	−1.741	0.208	0.113
0.169	0.233	−3.53	−0.031	1.24	7.61	−2.090	0.209	0.104
0.209	0.229	−6.78	−0.032	1.63	9.50	−2.515	0.211	0.090
0.249	0.222	−12.00	−0.033	2.06	11.72	−3.023	0.211	0.069
Configuration: prolate ABCF (−, 1)								
0.289	0.181	−26.80	−0.033	2.11	21.67	−3.929	0.180	0.010
0.329	0.180	−26.44	−0.036	2.52	22.95	−5.051	0.180	0.011
0.369	0.185	−26.95	−0.037	3.27	24.67	−6.243	0.185	0.010
Configuration: prolate AFef (−, 1)								
0.209	0.236	4.10	−0.035	7.31	8.55	−1.377	0.196	0.132
0.249	0.234	5.83	−0.036	7.67	9.67	−2.139	0.189	0.137
0.289	0.224	10.87	−0.039	8.24	10.66	−3.021	0.169	0.146
Configuration: prolate BE (−, 1)								
0.000	0.236	−0.08	−0.031	0.00	1.89	−1.079	0.204	0.118
0.050	0.241	−0.28	−0.030	0.34	2.71	−1.288	0.209	0.119
0.090	0.239	−0.71	−0.030	0.62	4.51	−1.474	0.208	0.117
0.130	0.237	−1.36	−0.030	0.91	6.03	−1.747	0.208	0.114
0.169	0.235	−2.23	−0.030	1.24	7.43	−2.094	0.208	0.110
0.209	0.234	−3.35	−0.030	1.63	8.78	−2.505	0.209	0.105
0.249	0.225	−9.88	−0.034	2.08	10.44	−2.993	0.211	0.077
0.289	0.228	−11.15	−0.036	2.73	11.59	−3.584	0.216	0.074
Configuration: prolate ABDE (−, 1)								
0.329	0.192	−16.76	−0.045	2.54	22.24	−4.507	0.187	0.044
0.369	0.191	−17.15	−0.046	3.16	23.57	−5.660	0.186	0.042
0.409	0.191	−16.05	−0.046	4.56	24.66	−6.860	0.185	0.046
Configuration: prolate BEef (−, 1)								
0.209	0.237	3.37	−0.035	7.27	8.50	−1.375	0.198	0.130
0.249	0.236	3.27	−0.036	7.62	9.77	−2.124	0.198	0.130
0.289	0.234	0.66	−0.038	7.71	11.42	−2.968	0.201	0.119
Configuration: prolate AH (−, 1)								
0.000	0.227	2.01	−0.030	0.00	2.28	−0.899	0.192	0.120
0.050	0.235	3.00	−0.030	0.31	2.82	−1.021	0.197	0.128
0.090	0.230	3.65	−0.030	0.53	4.51	−1.205	0.192	0.128
(0.130	0.226	3.54	−0.030	0.76	5.95	−1.469	0.189	0.125)
0.130	0.219	−9.98	−0.032	0.89	7.09	−1.474	0.206	0.075
0.169	0.212	−13.47	−0.033	1.18	9.02	−1.869	0.203	0.060
0.209	0.205	−16.93	−0.034	1.47	10.58	−2.320	0.200	0.046
0.249	0.201	−18.23	−0.036	1.80	12.29	−2.890	0.197	0.041
Configuration: prolate ABCH (−, 1)								
0.289	0.180	−23.59	−0.036	2.08	20.60	−3.771	0.179	0.020
0.329	0.182	−20.70	−0.040	2.44	21.60	−4.852	0.179	0.029
0.369	0.182	−23.60	−0.038	3.10	23.12	−5.978	0.181	0.020
Configuration: prolate AHef (−, 1)								
0.209	0.226	12.73	−0.033	7.77	8.40	−1.183	0.166	0.153
0.249	0.228	11.37	−0.034	7.98	9.55	−1.966	0.171	0.150
0.289	0.238	6.83	−0.039	7.89	11.09	−2.896	0.185	0.139

TABLE 6—continued

$\hbar\omega$ [MeV]	β_2	γ	β_4	I_{xZ} [$\hbar$]	I_{xN} [$\hbar$]	E' [MeV]	x	y
Configuration: prolate BG (−, 1)								
0.000	0.227	−0.75	−0.030	0.00	2.08	−0.877	0.198	0.111
0.050	0.238	1.88	−0.030	0.32	2.70	−1.019	0.202	0.126
0.090	0.235	2.12	−0.030	0.57	4.49	−1.202	0.199	0.125
(0.130	0.232	−0.20	−0.030	0.86	6.03	−1.466	0.201	0.115)
0.130	0.220	−9.98	−0.031	0.90	6.60	−1.477	0.207	0.075
0.169	0.218	−11.20	−0.031	1.22	7.81	−1.843	0.207	0.070
0.209	0.218	−12.57	−0.031	1.58	9.16	−2.275	0.208	0.065
0.249	0.222	−11.99	−0.033	2.05	10.49	−2.834	0.211	0.069
Configuration: prolate ABDG (−, 1)								
0.329	0.183	−16.67	−0.042	2.41	21.95	−4.351	0.178	0.042
0.369	0.187	−17.12	−0.042	3.09	23.07	−5.509	0.182	0.042
0.409	0.182	−16.38	−0.041	4.10	24.67	−6.652	0.177	0.043
Configuration: prolate BGef (−, 1)								
0.169	0.234	6.98	−0.033	7.06	6.91	−0.425	0.187	0.141
0.209	0.232	8.41	−0.034	7.51	7.99	−1.100	0.182	0.144
Configuration: oblate AF (−, 1)								
0.169	0.176	−60.83	−0.002	0.59	10.61	−1.518	0.151	−0.090
Configuration: oblate ABCF (−, 1)								
0.130	0.184	−55.59	0.004	0.51	19.59	0.189	0.166	−0.079
0.169	0.182	−56.93	0.004	0.66	20.42	−0.749	0.162	−0.082
0.329	0.162	−63.33	−0.002	1.62	23.06	−5.244	0.136	−0.089
Configuration: oblate AFef (−, 1)								
0.130	0.164	−91.72	−0.018	9.88	8.88	−0.235	0.078	−0.144
0.169	0.161	−90.13	−0.017	9.88	9.01	−1.075	0.080	−0.139
0.209	0.161	−89.39	−0.016	9.94	9.14	−1.932	0.082	−0.138
Configuration: oblate ABCFef (−, 1)								
0.289	0.146	−72.18	−0.006	9.44	21.96	−3.881	0.108	−0.098
0.329	0.153	−68.52	−0.006	10.30	22.52	−5.290	0.120	−0.095
Configuration: oblate BE (−, 1)								
0.169	0.180	−54.75	−0.002	0.68	8.65	−1.254	0.163	−0.075
0.209	0.187	−55.65	0.000	0.85	9.71	−1.727	0.168	−0.081
Configuration: oblate ABDE (−, 1)								
0.289	0.146	−82.60	−0.014	0.19	19.36	−3.436	0.088	−0.116
Configuration: oblate ABDEef (−, 1)								
0.289	0.172	−97.59	−0.018	9.98	21.72	−3.756	0.065	−0.159

increasing I) and by centrifugal stretching in the prolate ground band. Such "stretching", which also includes a transition towards more negative γ-values, is qualitatively supported by the calculations, and is a consequence of the soft energy minimum in the TRS of the vacuum configuration (see the two surfaces in the top row of fig. 6a).

A first band crossing in the nearly prolate band, corresponding to an alignment of a pair of $i_{13/2}$ neutrons (AB), is predicted by the calculations to appear at $\hbar\omega \approx 0.25$ MeV. Since the Fermi surface lies in the upper part of the $\nu i_{13/2}$ shell, this triggers a change to negative γ-values ($\sim -15°$). In fig. 7a these points are labelled "AB" and are seen to be more localized in γ as a function of $\hbar\omega$ than the

values before the crossing. The calculations also show that at higher rotational frequencies a second neutron pair will align in the yrast band to form the ABCD configuration, for which γ remains at about $-15°$ but β_2 is reduced relative to the AB band (see table 6). The deformation of the AB and ABCD configurations is more stable than that of the vacuum configuration (g-band), and the corresponding minima in the TRS surfaces are stiffer, in particular in the ABCD configuration (cf. fig. 6a). At higher rotational frequencies the four-quasiparticle band $(\nu i_{13/2})^2 \otimes (\pi h_{9/2})^2$ (ABef) will also lie relatively low in energy. The proton Fermi surface is close to the $K = \frac{1}{2}$ level of the $h_{9/2}$ shell, and therefore the alignment of the $\pi h_{9/2}$ pair drives the deformation from $\gamma \approx -15°$ (configuration AB) back to a more prolate shape but the energy minimum is very soft in the γ-direction (cf. fig. 6a), and as the rotational frequency increases in this band the γ-deformation becomes more negative. According to the calculations the ABef band never comes sufficiently low in energy to form a part of the yrast line.

6.1.2. Band 2. As discussed earlier, band 2 can be associated with the configuration $\pi i_{13/2} \otimes \pi h_{9/2}$, here denoted af. In both shells the Fermi surface is near the $K = \frac{1}{2}$ level and a polarizing effect towards larger β_2 values and positive γ-values can be expected. This is confirmed by the calculations which give $\beta_2 \approx 0.25$ and $\gamma \approx 10°$ (figs. 6b, 7b and table 6). Since the $\pi h_{9/2}$ alignment is blocked, the first band crossing is due to $i_{13/2}$ quasineutrons. Due to the polarizing effect of the $\nu i_{13/2}$ pair, both β_2 and γ are slightly decreased above the band crossing, but the change is small due to the dominanting influence of the $\pi i_{13/2}$ orbital. The TRS is, however, very soft in the γ-direction (see fig. 6b, configuration ABaf) and quite similar to that of the ABef configuration (fig. 6a) in which negative γ-values were obtained.

6.1.3. Bands 3-6. These bands are all expected to have the configuration $\nu i_{13/2}$ coupled to either a $\nu f_{7/2}$ or $\nu p_{3/2}$ quasiparticle. The observed bands in ^{183}Pt [ref. [16])] and ^{185}Pt [ref. [17])] and theoretical quasiparticle energy diagrams, like those discussed in sect. 6.2, show that several negative-parity neutron levels (E, F, G, etc.) lie very close in energy just above the Fermi surface, implying the existence of a number of close lying negative pairty bands (AE, AF, AG, BE, etc.). It is therefore not completely obvious which ones of the theoretical configurations will correspond to the observed bands, although the suggestion is made in fig. 7c, d that the configurations AE and AF correspond to band 3 and 4, respectively. At low frequencies these configurations (as well as the configurations BE and BF) have the $[624]^{9+}_{2} \otimes [514]^{7-}_{2}$ structure suggested for the experimental bands 3 and 4. The single-particle structure of the excited configurations labelled AG, AH, BG and BH is less well defined, since it undergoes major changes already at low frequencies as the deformation abruptly goes from prolate to triaxial. This is most clearly seen in the configurations AH and BG, which have coexisting minima at $\gamma \approx 0°$ and $-10°$ for $\hbar\omega = 0.13$ MeV (see table 6).

Independent of the structural differences, all the calculated negative-parity bands undergo similar deformation changes. Four of the lowest bands of each signature

are included in fig. 7 and in table 6. The deformations of these bands lie close to $\beta_2 = 0.23$ before the first band crossing, but γ is changing from about 0° near the bandhead to about −10° or −15° just before the first band crossing, which is calculated to be the BC or AD crossing depending on the signature of the excited $i_{13/2}$ neutron. Above the band crossing the γ-deformation becomes even more negative with values ranging from −15° to −30°. A comparison between figs. 7c and 7d shows that it is the negative-parity neutron that determines the precise deformation of the negative-parity four-quasiparticle (4qp) neutron bands. In these bands β_2 is less than 0.20, which is significantly smaller than that in the 2qp bands. The TRS plots of the AF and ABCF configurations are shown in fig. 6b.

We have also calculatd the deformation of the 4qp bands which contain an aligned proton pair (ef) instead of the neutron BC or AD pair. These bands lie higher in energy than the 4qp neutron bands and have deformations with $0° < \gamma < 15°$ and $\beta_2 \approx 0.24$. Also in this case, it is the negative-parity neutron which determines the precise deformation and how it changes with increasing frequency (see fig. 7 and table 6).

6.1.4. Other structures. Fig. 7 also shows several configurations of predominantly oblate shapes. Of these only the lowest lying oblate band has been observed [9]), starting from a 0^+ state at 492 keV. In the present experiment only the 2^+ and 4^+ states are seen (band 8). However, candidates for several of these other configurations have been observed in the $N = 108$ nuclei, e.g. ^{186}Pt [ref. [21])] and in Hg isotopes with $N \geq 106$ (e.g. refs. [42,44])).

In the oblate configurations the strong polarizing effect of aligned protons must be mentioned. Whereas practically all pure neutron configurations have γ-values in the range $-75° < \gamma < -50°$, most of the configurations with an aligned proton pair (ef) have deformations with $\gamma < -75°$. The β_2 values for the oblate bands usually lie between 0.15 and 0.18, whih is considerably smaller than for the prolate bands.

It should also be pointed out that for oblate shapes the aligning proton pair does not originate from the $h_{9/2}$ subshell, which is the case for prolate shapes, but rather from the $h_{11/2}$ subshell. This is because the Fermi surface lies among the low-K orbitals in the top of the $h_{11/2}$ subshell for an oblate shape.

Large-deformation bands ($\beta_2 \approx 0.425$, $\gamma \approx 0°$) are predicted to come near the yrast line at $\hbar\omega \geq 0.30$ MeV, becoming yrast at $\hbar\omega \approx 0.6$ MeV. The associated configurations contain two aligned $i_{13/2}$ protons and two $j_{15/2}$ neutrons. Minima corresponding to such highly deformed bands can be seen in some of the TRS surfaces in figs. 6a and 6b.

6.2. THEORETICAL INTERPRETATION OF BAND CROSSINGS AT $N = 106$ AND $N = 107$

As seen from fig. 7 and table 6, the low-lying bands in ^{184}Pt may have deformations ranging practically from $\gamma = -30°$ to $\gamma = 15°$. In addition, higher lying "oblate" bands have γ-values between −90° and −50°. In such extreme situations blocking

arguments cannot be used, since the band-crossing frequency changes rapidly with the deformation. To quantify this effect, we have performed Woods-Saxon cranked-shell-model (CSM) calculations for different sets of deformation and pairing parameters. Examples of the resulting CSM diagrams are illustrated in fig. 8 for three different values of γ, namely $\gamma = +15°$ which is representative of certain configurations in which the strongly deformation driving $h_{9/2}$ and/or $i_{13/2}$ protons are excited, $\gamma = 0°$ representing the prolate deformations calculated for most bands at low frequencies near the bandhead, and $\gamma = -15°$ which is a typical deformation for many configurations with aligned $i_{13/2}$ neutrons. Diagrams are shown both for protons and neutrons, with pairing gaps relevant to the first band crossing (ef for protons and AB for neutrons). Of special interest here is the trend of the crossing frequencies for $\nu i_{13/2}$ and $\pi h_{9/2}$ alignment processes. These values of the crossing frequencies are extracted from the CSM diagrams (like those in fig. 8) and collected in fig. 9.

It is clear from fig. 9 that all neutron crossing frequencies become very low for negative γ-values. For small positive γ-values, they stay relatively constant at values that are slightly larger than for a pure prolate shape, and for $\gamma > 10°$ they may even start to decrease. The first proton crossing frequency, ω_{ef}, is always higher than the lowest neutron crossing frequency, ω_{AB}, even for positive γ-values where ω_{AB} has a maximum and ω_{ef} is minimized (assuming full proton pairing). For negative γ values, the proton crossing frequency increases rapidly and for $\gamma < -5°$ is even higher than the CD neutron crossing frequency. As seen from fig. 9, the crossing frequencies may easily change by 0.1 MeV or more over the γ-interval covered by the figure, which necessarily has to be taken into account when analyzing the experimental band-crossing frequencies. Furthermore, the neutron and proton numbers have a large influence on the crossing frequencies. In particular at $N = 108$ the neutron-crossing frequency changes dramatically, getting a much stronger γ-dependence, which has to be kept in mind in the analysis below. Also the pairing gap has a strong influence on the crossing frequencies. In fig. 9 the different pairing gaps have been calculated using Δ-values which are reasonable average values for the crossing bands, determined from pairing self-consistent calculations (for details see the figure caption). For the proton ef crossing, an extra curve is included representing a situation when the proton pairing is reduced by the presence of an excited odd proton (the dotted curve). It is clear that fig. 9 only shows the qualitative features and that it should not be used for extracting quantitative values. In particular when crossing bands have different deformations, only a very rough estimate of the actual band-crossing frequency can be made, for example by taking the average deformation of the bands. For a more detailed discussion of such band crossings, we refer to ref. [48]).

Based on the behavior of the crossing frequencies shown in fig. 9 and the calculated deformations shown in fig. 7, the observed band crossings can be given a precise interpretation, as shown below. We then discuss the different types of bands in the

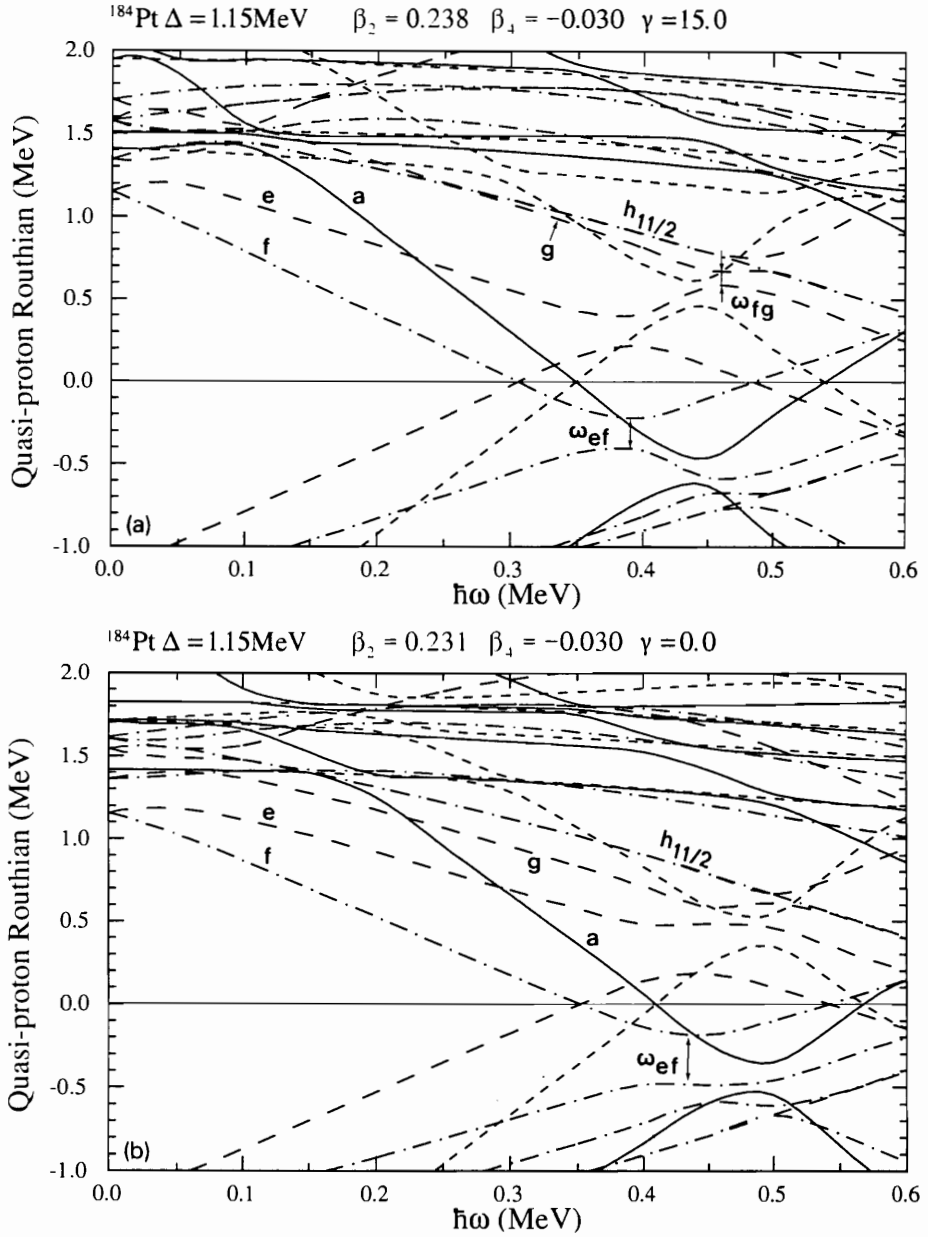

Fig. 8. (a)-(c) Calculated quasiparticle energy diagrams for protons in ^{184}Pt at $\gamma = +15°$, 0° and −15°. The β_2 and β_4 values are chosen to be representative for configurations with an energy minimum at the corresponding γ-value. The pairing gap is appropriate at the first band crossing (ef). The Fermi energy is kept fixed at a value which gives the correct proton number at $\hbar\omega = 0.0$ MeV. Low-lying quasiparticle levels are labelled according to the convention defined in table 3, and band crossings discussed in the text are indicated. It is clear that the crossing frequencies in these diagrams depend strongly on γ. (d)-(f) Same as (a)-(c) but for neutrons. The pairing gap is representative for the first band crossing (AB), and the Fermi energy is kept constant at a value which gives the correct neutron number at $\hbar\omega = 0.0$ MeV.

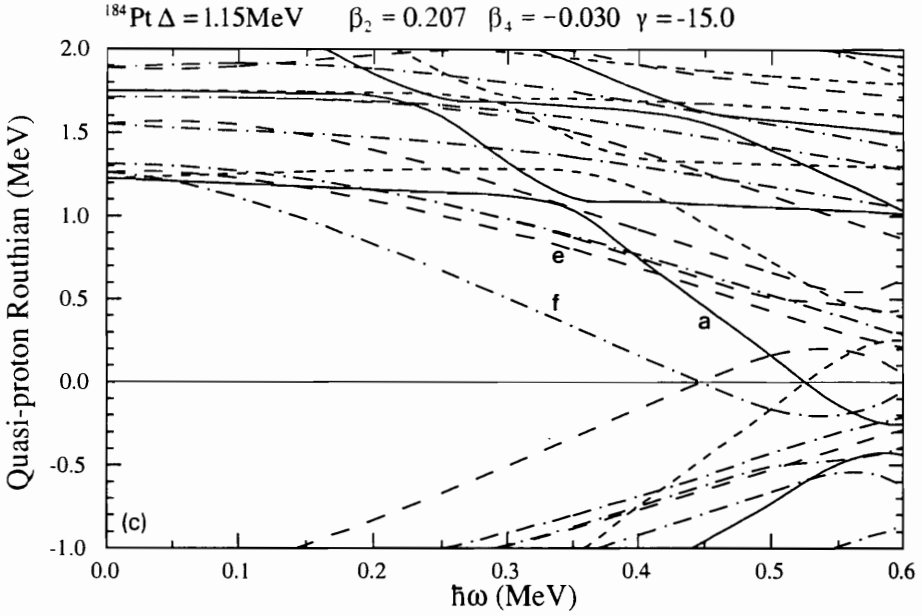

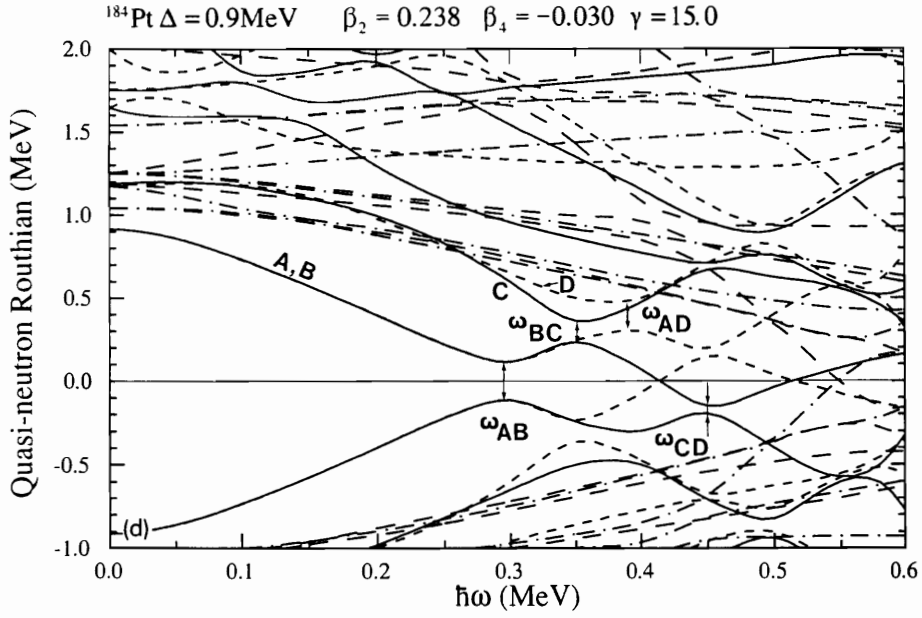

Fig. 8—continued

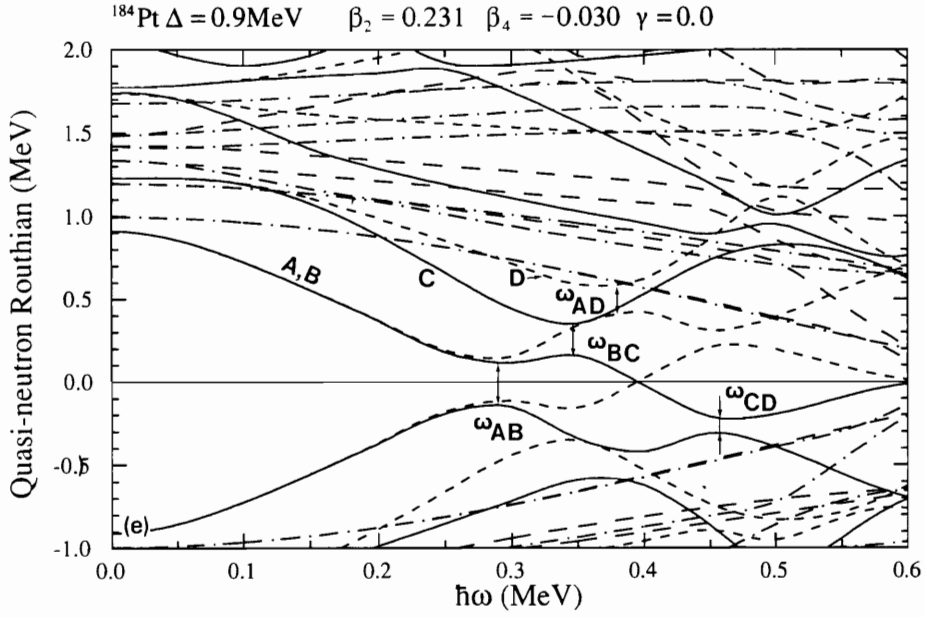

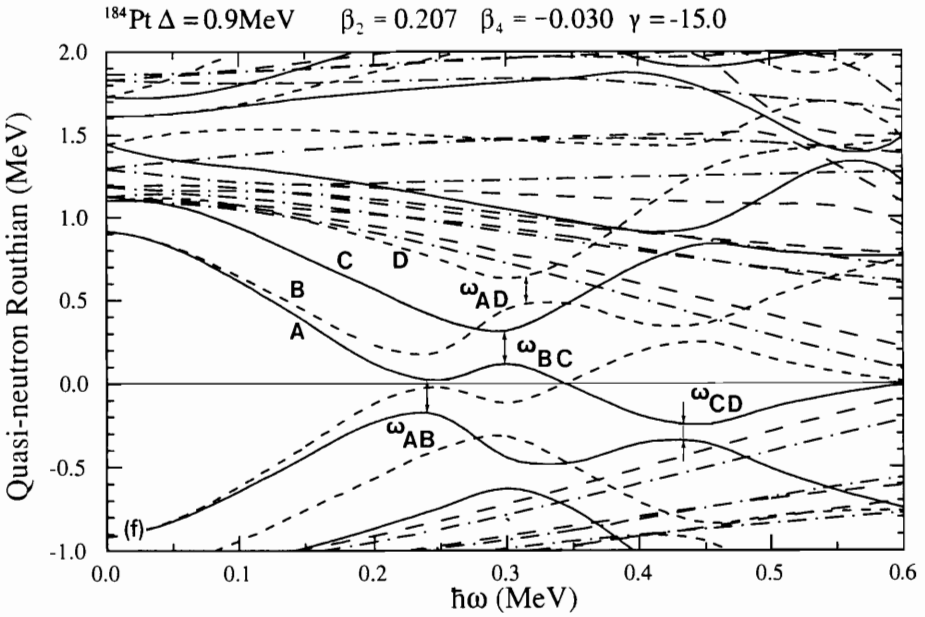

Fig. 8—continued

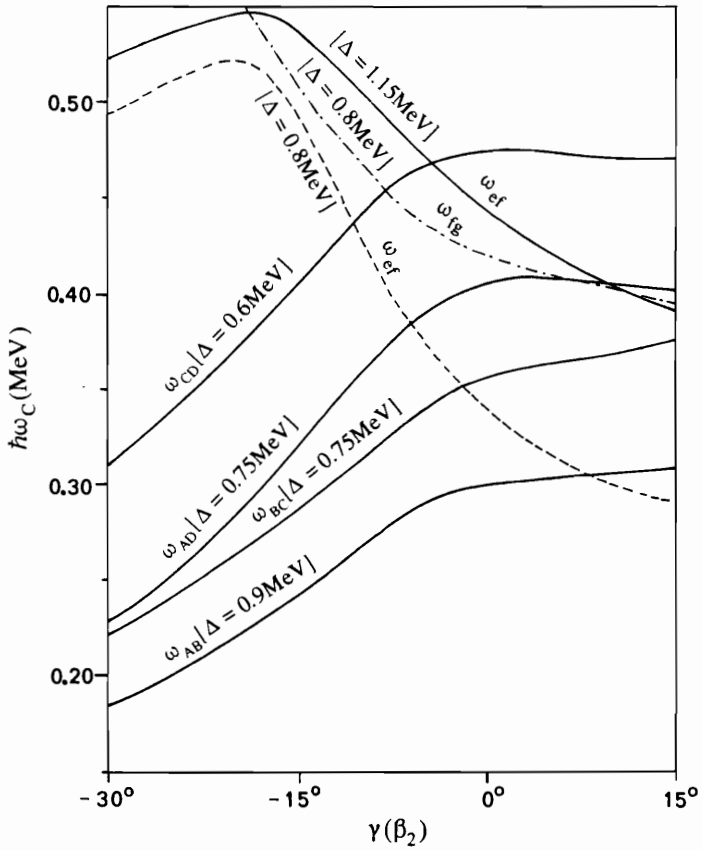

Fig. 9. Band-crossing frequencies determined from quasiparticle diagrams similar to those in fig. 8. Different pairing gaps and Fermi energies, representative of the individual crossings, have been used. The plot is drawn as a function of γ, but also β_2 has been varied slightly to define a trajectory which goes through the equilibrium deformation points (see fig. 7). A constant value of $\beta_4 = -0.03$ was used. The figure also shows ef proton crossing frequencies calculated with a reduced pairing gap (short-dashed lines).

same order as they were presented in sect. 4. The quasiparticle assignments for the crossings are summarized in table 5.

6.2.1. Bands with an excited $i_{13/2}$ neutron, in which the AB neutron crossing is blocked. This kind of band is represented by negative-parity side bands in even-even nuclei and by $\nu i_{13/2}$ bands (A and B bands) in odd-N nuclei. The first unblocked crossing is either the neutron BC (or AD) or the proton ef crossing. These bands typically have a nearly prolate deformation near the bandhead, but the deformation changes gradually towards negative γ-values as the $i_{13/2}$ neutron gets more aligned, reaching a γ value of about $-10°$ to $-15°$ just before the first band crossing. At these γ values only neutrons can align (BC or AD crossing) below $\hbar\omega = 0.35$ MeV. The lowest proton crossing (ef) is predicted to lie at $\hbar\omega \approx 0.50$ MeV. Only for positive

γ-values will the ef crossing appear at similar frequencies as the BC and AD crossings, but such deformations are never favored in configurations with an excited $i_{13/2}$ neutron. After the BC or AD pair has aligned, γ becomes even more negative, lying typically between $-15°$ and $-30°$. In bands with an excited $i_{13/2}$ neutron we therefore expect to see a single band crossing below $\hbar\omega = 0.35$ MeV, corresponding to an alignment of the BC or the AD pair depending on the signature. The negative-parity neutron side bands in ^{184}Pt and the A and B bands in ^{185}Pt, which are examples of such bands, all have crossings below $\hbar\omega = 0.3$ MeV.

6.2.2. Bands with an excited $h_{9/2}$ proton in which the ef crossing is blocked. This kind of band is represented by $h_{9/2}$ bands (e- or f-bands) in odd-Z nuclei and by certain sidebands in even-even nuclei, e.g. the af band in ^{184}Pt. The first unblocked band crossing is expected to be the AB neutron crossing, since the lowest unblocked proton crossing (eh or fg) can hardly come below 0.4 MeV at any γ-value even if the proton pairing gap is strongly reduced by the presence of an excited proton. In particular the eh crossing, which appears in the favored band (f), lies at a very high frequency. This is because we are not dealing with a single high-j subshell, but with the combined $h_{9/2}$ and $f_{7/2}$ subshells. The lowest quasiparticle levels originating from these subshells will therefore appear in the order $\alpha = \frac{1}{2}, -\frac{1}{2}, -\frac{1}{2}$ and $\frac{1}{2}$. Excluding the high-K levels from the $h_{11/2}$ subshell, the corresponding letter notations become f, e, g and h. With this level order, the fg crossing will have a comparatively low frequency (cf. fig. 9) while the eh-crossing will appear at a very high frequency. Actually $\omega_{eh} > 0.55$ MeV/$\hbar$ even for a small pairing gap of $\Delta = 0.8$ MeV, which explains why this crossing does not appear in fig. 9. The properties of the quasiparticle levels and band crossings referred to above are clearly illustrated in figs. 7a and 7b. Bands with an excited $h_{9/2}$ proton usually have a deformation with γ close to zero or positive. At such deformations the neutron AB crossing appears at a frequency close to 0.30 MeV. No other band crossing is possible below $\hbar\omega = 0.35$ MeV. The prediction agrees with the experimental observations of crossings in the f band in ^{183}Ir and ^{185}Au and in the af band in ^{184}Pt: a single band crossing is expected below $\hbar\omega = 0.35$ MeV and it is caused by the alignment of the neutron AB pair.

6.2.3. Bands with both an excited $i_{13/2}$ neutron and an $h_{9/2}$ proton, in which both the AB and the ef crossings are blocked. Bands of this kind appear at low energies in odd-odd nuclei like ^{186}Au and ^{184}Ir, the most favored bands being Af and Bf. The first unblocked neutron crossing is the BC (or AD) alignment and the first unblocked proton crossing is eh (or fg). The calculations show, however, that the BC and AD alignment processes appear at a lower frequency independent of the deformation, and therefore the first crossing has to be due to a neutron pair. Since the $i_{13/2}$ neutron and the $h_{9/2}$ proton have opposite deformation-driving forces, the deformation in most cases stays close to $\gamma = 0$ before the first band crossing. Both the BC and AD crossings are expected to lie above $\hbar\omega = 0.35$ MeV, although the former crossing may lie close to this frequency if γ is slightly negative. In any case the first band crossing in such an odd-odd structure will appear at a much higher

frequency than in the A and B bands where the same neutron crossings appear, but where $\gamma \ll 0$. Therefore, the γ dependence of the BC crossing can explain both the low frequency crossing ($\hbar\omega = 0.25$ MeV) in the A-band of ^{185}Pt ($\gamma \sim -15°$) and the absence of a crossing below $\hbar\omega = 0.35$ MeV in the Af bands of ^{184}Ir and ^{186}Au ($\gamma \sim 0°$). This is summarized in table 5.

6.2.4. Bands without excited $i_{13/2}$ neutrons or $h_{9/2}$ protons in which no band crossings related to high-j subshells are blocked. Bands of this kind are the ground bands in even-even nuclei, positive-parity bands in odd-Z nuclei, and negative-parity bands in odd-N nuclei. The lowest band crossing must be either the neutron AB or the proton ef crossing, the relative positions of which strongly depend on the deformation. The calculations show that most configurations, which do not have excited particles in the proton $i_{13/2}$ orbital (or the $h_{9/2}$ orbital, discussed in sect. 6.2.2), develop deformations with negative γ-values before the first band crossing. In such cases the first band crossing has to be due to neutrons according to fig 9. Even in configurations with positive γ-values, of which the proton $i_{13/2}$ band (a) is one of the few good examples, the neutron AB crossing is predicted to lie below the proton ef crossing. However, if we take into consideration that the odd proton (in this case a) reduces the proton pairing gap, thereby also reducing the proton crossing frequency, it can be expected (see fig. 9) that both protons and neutrons align at nearly the same frequency. This theoretical analysis then agrees with the way in which the experimentally observed proton $i_{13/2}$ band in ^{185}Au has been interpreted by Larabee *et al.*[3]): $\nu i_{13/2}$ and $\pi h_{9/2}$ crossings at nearly degenerate frequencies.

However, the majority of the bands have negative γ-values (typically after the first band crossing (AB) $\gamma \leqslant -15°$), and thus the first proton crossing (ef) lies very high ($\hbar\omega \geqslant 0.5$ MeV) even if the proton pairing is reduced. It therefore cannot be involved in any band crossing in the experimentally observed frequency range [except for those structures involving the $\pi i_{13/2}$ (a) orbital]. Nevertheless many of the observed band crossings are associated with a gain in angular momentum too large to be explained by just the AB neutron pair. In some cases the experimental data even give evidence for two reasonably well separated alignment processes (e.g. the $\pi d_{5/2}$ band in ^{183}Ir). The calculations give a natural explanation to these observations. At large negative γ-values ($\approx -15°$) the second neutron crossing (CD) comes down to frequencies as low as those calculated for the first proton crossing (ef) at positive γ-values (if the proton pairing is not reduced by excited protons). Indeed at $\gamma \approx -30°$ the CD crossing may be almost as low as 0.30 MeV if the neutron pairing gap is reduced to 0.6 MeV, which is a reasonable value at this crossing. For large negative γ-values, the CD crossing lies far below the ef crossing, even if the proton pairing is strongly reduced. Both the frequency and the interaction strength of the CD crossing varies markedly with both deformation and particle number, but this crossing appears typically between $\hbar\omega = 0.35$ MeV and 0.40 MeV and is usually associated with a relatively large interaction strength. A particularly low

CD crossing with comparatively small interaction is calculated for ^{183}Ir, where the double band crossing observed in the $\pi d_{5/2}$ band is well described by the calculations. In other cases the CD pair is expected to align more gradually over a wide frequency range continuing the alignment process started by the AB pair, but not giving rise to a sharp enough band crossing to be easily identified in the experimental data. The full alignment may not be reached until $\hbar\omega \approx 0.4$ MeV or more. However, this is still well below the proton ef crossing. The yrast band in ^{184}Pt may be given this explanation, and quite generally it can be concluded that the CD crossing appears in the calculations at about the right frequency to account for the excess alignment acquired by the nucleus in close connection to or shortly above the AB crossing.

In conclusion, the calculations suggest that two alignment processes take place in a frequency interval starting at $\hbar\omega \approx 0.20$ MeV and ending at $\hbar\omega \approx 0.40$ MeV. In most cases (bands with $\gamma \ll 0°$) the aligning particles are the AB and CD neutrons: the $\pi d_{5/2}$ band of ^{183}Ir; the yrast band of ^{184}Pt; bands E, F, and H of ^{185}Pt. In the last three cases, the existing experimental data do not reach sufficiently high frequencies to confirm the existence of a double crossing. In exceptional cases (bands with $\gamma > 0°$ and reduced proton pairing) the aligning particles could be the AB neutrons and the ef protons, like in the $\pi i_{13/2}$ band of ^{185}Au. This then presents the curious scenario where apparently identical band crossings in the yrast band of ^{184}Pt and the $\pi i_{13/2}$ band of ^{185}Au result from different alignment processes.

6.3. THEORETICAL INTERPRETATION OF BAND CROSSINGS AT $N = 108$

The band crossing pattern for the $N = 108$ isotones deviates significantly from that discussed for the $N = 106$ and $N = 107$ isotones in sect. 6.2, as can be seen from a careful consideration of fig. 4. This change results mainly from the fact that a gap at 108 in the neutron single-particle spectrum causes the neutron Fermi energy to increase significantly at prolate shapes to a position just between the $\Omega = \frac{9}{2}$ and $\Omega = \frac{11}{2}$ levels of the $i_{13/2}$ subshell. As a result, the neutron AB crossing is increased in frequency to around 0.4 MeV. The $N = 108$ gap is a prolate structure, which does not appear at deformations with $\gamma \leq -15°$. For such negative γ-deformations the $i_{13/2}$ neutrons still align at a very low frequency, e.g. $\hbar\omega_c(\mathrm{AB}) \approx 0.2$ MeV. The main difference compared to the $N = 106$ and 107 isotones is that the neutron crossings in the $N = 108$ isotones have a much stronger γ-dependence than shown in fig. 9. The consequences for the bands shown in fig. 4 are discussed below.

6.3.1. The proton $h_{9/2}$ bands in ^{185}Ir and ^{187}Au. Both bands are calculated to have a near prolate deformation and therefore the neutron AB crossing is expected to lie at $\hbar\omega \approx 0.4$ MeV. The first band crossing is in fact observed at this frequency. In ref. [25]), however, it was suggested that this band crossing in ^{185}Ir is due to the first unblocked proton alignment (eh). This possibility is, however, ruled out by the calculations, which show that an eh crossing below $\hbar\omega \approx 0.55$ MeV is not possible

(see sect. 6.2.2, cf. also fig.8a), and therefore the observed band crossing must be the AB alignment. The same is expected for the af band in ^{186}Pt, but here the experimental data do not reach sufficiently high frequencies to reveal the position of the first band crossing.

6.3.2. The proton $i_{13/2}$ band in ^{187}Au. As for the corresponding band in ^{185}Au, the deformation for the $\pi i_{13/2}$ band in ^{187}Au has $\gamma > 0$, and the proton pairing is reduced. Therefore, the proton ef pair is expected to align at a low frequency (<0.3 MeV). Due to the positive γ-values, the neutrons (AB) are not expected to align below $\hbar\omega \approx 0.4$ MeV. In contrast to the $\pi i_{13/2}$ band in ^{185}Au, where most likely both the ef protons and the AB neutrons align below $\hbar\omega \approx 0.35$ MeV, only one band crossing (ef) is expected to occur below ~0.4 MeV in ^{187}Au. The experimental data show that this is actually the case.

6.3.3. The g-band in ^{186}Pt and the $\pi d_{5/2}$ band in ^{185}Ir. In these configurations there are no particles excited (protons $h_{9/2}$ or $i_{13/2}$) which can stabilize the deformation at $\gamma \geq 0°$. Already before any particles align, γ is negative and according to the calculations the first particles to align are the AB neutron pair, which drives the deformation to very large negative γ-values ($\gamma \approx -30°$ in the S-band of ^{186}Pt). Calculations, which take the sizable deformation change at the band crossing into account, suggest that the AB alignment should be observed at a frequency between 0.20 and 0.25 MeV, in good agreement with the experimentally observed band-crossing frequencies. The calculations also give a natural explanation of the band crossings observed in the g-band of the $N = 108$ isotones ^{184}Os ($\hbar\omega \approx 0.31$ MeV) and ^{182}W (possibly an onset of alignment at $\hbar\omega \approx 0.4$ MeV). In ^{182}W the calculated neutron S-band has a nearly prolate shape and the AB crossing is not expected below ~0.4 MeV. In ^{184}Os the S-band has moderately large negative γ-values, and an AB band crossing at a frequency in between that of ^{186}Pt and ^{182}W is expected.

In conclusion the calculations allow for a consistent interpretation of the $N = 108$ isotones, in addition to that of the $N = 106$ and 107 isotones discussed above. The unique feature of the $N = 108$ isotones is the large changes (nearly a factor of two) in the AB neutron crossing frequency, which appear as a result of the large difference in deformation between different configurations.

6.4. THEORETICAL CONDITIONS FOR THE APPEARANCE OF BANDS WITH AN ALIGNED PROTON $h_{9/2}$ PAIR

In sect. 5 an interpretation of the observed band crossings in the $N = 106$, 107, and 108 isotones was made based on standard blocking arguments. This requires the assumption that the deformation is approximately the same (in practice prolate) for all the bands, so that deformation-related variations in band crossing frequencies can be avoided. The assumption of a common prolate deformation is obviously not consistent with the calculations, which predict that all configurations with one or

more excited $i_{13/2}$ neutrons will develop deformations with $\gamma < 0°$, at least for frequencies in the band crossing region. We may, however, assume for a moment that the calculated deformations are not correct and that the deformation stays close to $\gamma = 0°$. Will the conclusions drawn in sect. 5 then be reasonable?

There are three major differences between the interpretation presented in sect. 5 based on blocking arguments and in sect. 6 based on the theoretical calculations:

(i) All band crossings which theoretically were interpreted as resulting from the alignment of BC or AD neutrons are thought in the blocking interpretation to be caused by an alignment of the ef protons. This difference in interpretation appears for the neutron $i_{13/2}$ bands in odd-N nuclei (e.g. ^{184}Ir and ^{185}Pt) and for the negative-parity neutron side bands in the even-even nuclei (e.g. ^{184}Pt).

(ii) All band crossings which theoretically were suggested to involve the neutron CD pair are proposed, in the blocking interpretation, to have the proton ef pair aligning instead. This difference affects mainly the g-band in the even-even nuclei (e.g. ^{184}Pt) and most of the positive-parity bands in the odd-Z nuclei (e.g. $\pi d_{5/2}$ in ^{183}Ir and ^{185}Ir).

(iii) In the $N = 108$ isotones, the blocking arguments suggest that all band crossings below $\hbar\omega \approx 0.4$ MeV are due to ef protons and never due to AB neutrons as theoretically predicted for the g-band in ^{186}Pt and for the $\pi d_{5/2}$ band in ^{185}Ir.

We have calculated the deformation for those aligned bands resulting from replacing the BC, AD, or CD neutron pair with an ef proton pair. The results are shown in fig. 7 and table 6, along with the values for the proton S-band (ef). With one exception all of these bands have deformations with γ between 0° and 15°. Only the ABef band has $\gamma < 0°$. With some approximation we may say, however, that these bands are essentially prolate. In any case they deivate less from prolate shape than the bands with aligned BC, AD or CD neutrons.

An essential feature of the blocking arguments used in sect. 5 is that the proton ef crossing appears at a lower frequency than the neutron BC and AD crossings. A quick glance at fig. 9 shows that the BC crossing is always calculated to lie lower than the ef crossing, even for positive γ-values. In order to lower the frequency of the ef crossing, one must reduce the proton pairing. The ef crossing frequency, calculated with a reduced proton pairing gap ($\Delta = 0.8$ MeV) is shown by the dashed curve in fig. 9. Even with this reduced pairing gap, the proton ef crossing comes just barely below the neutron AB crossing at prolate shape. *Assuming slightly positive γ-values (5°-10°) and a reduced proton pairing ($\Delta_p = 0.8$ MeV)*, we find that the calculated crossing frequencies may be compatible with the scenario based on blocking arguments outlined in sect. 5:

(i) In bands with an excited $i_{13/2}$ neutron, where the AB crossing is blocked, there is only one crossing below $\hbar\omega \approx 0.35$ MeV, namely the proton ef crossing.

(ii) In bands with an excited $h_{9/2}$ proton where the ef crossing is blocked, the only crossing below 0.35 MeV is the neutron AB crossing.

(iii) In bands with both an excited $i_{13/2}$ neutron and an excited $h_{9/2}$ proton where both the AB and ef crossings are blocked, there will be no band crossing below $\hbar\omega \approx 0.35$ MeV.

(iv) In bands without excited $i_{13/2}$ neutrons and $h_{9/2}$ protons, both the AB neutrons and the ef protons will align at similar frequencies below 0.35 MeV.

To these points should be added that for $N = 108$ the neutron AB crossing is shifted to above $\hbar\omega = 0.35$ MeV, and therefore only the proton ef crossing will appear below this frequency.

The interpretation of the band crossings made above is in full agreement with the blocking scenario of sect. 5, and thus also consistent with the experimental data shown in fig. 4. However, two assumptions must be made, which have no support from the theoretical calculations:

(i) All the rotational bands have a deformation with slightly positive γ-values, implying that the $i_{13/2}$ neutrons do not drive the deformation to negative γ-values.

(ii) The proton pairing gap must be about 30% smaller than calculated, since this is the only way to get the ef crossing below the BC and AD crossings, to frequencies comparable with that of the AB crossing.

6.5. THEORETICAL SUMMARY

The theoretial calculations show that the rotational bands in ^{184}Pt and neighboring nuclei have a variety of deformations, which sometimes change significantly within a band. The calculations also show that the band-crossing frequencies are strongly deformation dependent, and that not even a rough estimate of a crossing frequency can be made unless the deformations of the crossing bands are known.

The band-crossing frequencies determined at the calculated deformations form a pattern which is fully consistent with the behavior of the experimentally observed crossing frequencies in the mass region around ^{184}Pt, suggesting that almost all of the observed band crossings are due to the alignment of $i_{13/2}$ neutrons. The only exceptions are bands having a deformation with $\gamma \geq 0^\circ$ and a reduced proton pairing, in which an alignment of $h_{9/2}$ protons is expected to take place below $\hbar\omega \approx 0.30$ MeV. Of the experimentally observed band crossings, only three occur in bands of this kind (the $\pi i_{13/2}$ bands in ^{185}Au and ^{187}Au and the $\pi i_{13/2} \otimes \nu i_{13/2}$ band in ^{186}Au).

The scenario based on blocking arguments presented in sect. 5 can only be theoretically reproduced if it is assumed that all bands have deformations with $0^\circ \leq \gamma \leq 10^\circ$ and that the proton pairing is strongly reduced in all bands. Neither of these assumptions are, however, supportd by the calculations, although the particular bands which have an aligned proton $h_{9/2}$ pair (ef), and which play a crucial role in the blocking scenario in most cases actually have a deformation in the interval $0^\circ \leq \gamma \leq 10^\circ$. Their calculated energy is, however, too high to make them likely candidates for the experimentally observed bands.

The inherent assumption in the theoretical calculations of sect. 6 is that the configurations are pure. For example, a particular band crossing occurs from one well-defined configuration and deformation to another. While there is no doubt about the deformation-driving tendencies of the various high-j orbitals and the concomitant variation of crossing frequencies with nuclear shape changes, the quantitative conclusions may change if the assumption of pure configurations is not correct. Attempts to calculate the dynamical aspects of the nuclear shape in band crossings have been made using the generator coordinate method (GCM) [45]. In this approach, the Hill-Wheeler equation is numerically solved by discretizing the collective variables and calculating the overlap matrix. Such a calculation is able then to trace the dynamical movement of the shape of the nucleus from one TRS minimum to another, as a function of rotational frequency. A key question presented in this paper is the competition between the ground configuration in ^{184}Pt ($\gamma \approx -3°$), the aligned $\nu i_{13/2}$ band ($\gamma \approx -15°$), and the aligned $\pi h_{9/2}$ band ($\gamma \approx 5°$). The actual crossing between the ground band and one or both of these aligned structures is a very sensitive function of the shape parameters, according to the static TRS calculations presented here. The next step is to perform the GCM calculations to see if the conclusions are altered by inclusion of the dynamical competition between these shapes. Such calculations are now being performed by Zhang *et al.* [46].

7. Summary

In summary, ^{184}Pt lies in a transitional mass region of soft nuclei where individual quasiparticles polarize the nuclear shape in different ways, leading to large shape variations. This point is well illustrated in fig. 7 where it is shown that the calculated equilibrium deformations for different bands cover a considerable part of the (β_2, γ) plane. (It should also be noted that large variations in β_4 as a function of configuration were also apparent in the calculations; see table 6.) Of the six observed side bands, one (band 2) is assigned to be based on a two-quasiproton configuration and four (bands 3-6) to two-quasineutron structures. Calculations suggest that these latter bands have rather negative equilibrium γ values, while the former should have positive γ. Transitions observed between bands 2 and 5 allow an extraction of the mixing matrix element, which is small and consistent with the different structures proposed for these bands. It also has been suggested that band 7 has a $(\nu i_{13/2})^2$ configuration built on a quasivibrational structure, but this assignment is the least certain of the six side bands and is based solely on systematics.

In this paper is presented (see fig. 4) the pattern of band crossings in nine nuclei in the vicinity of ^{184}Pt. The key question in this region has been whether the alignment of a proton $h_{9/2}$ pair can be responsible for band crossings below $\hbar\omega = 0.3$ MeV. We present here two complete but distinct scenarios for explaining the pattern of band crossings in these nine nuclei. The first is based on (a) blocking arguments

which assume similar shapes for the crucial bands, and (b) a measurement of the $B(M1)/B(E2)$ ratios in the $[624]^{9+}_{\frac{1}{2}}$ band of ^{185}Pt and the $[402]^{5+}_{\frac{5}{2}}$ band of ^{183}Ir [ref. [18])]. This approach results in the conclusion that a $\pi h_{9/2}$ band crossing occurs at $\hbar\omega \leq 0.3$ MeV in each of these nine nuclei ($N = 106$–108, Ir to Au).

Such a conclusion of a low-lying $\pi h_{9/2}$ crossing is mostly incompatible with the results of the second scenario, which is based on calculations of the nuclear shapes in different bands and the expected crossing frequencies. In this approach, it is only in bands containing $\pi i_{13/2}$ (which drives the nucleus to distinctly positive γ) that a low-frequency $\pi h_{9/2}$ crossing can occur. In other bands in these nine nuclei, the configuration minimizes at $\gamma < 0°$, which is not conducive to a low-frequency $\pi h_{9/2}$ crossing. Instead, many observed crossings are assigned to secondary $\nu i_{13/2}$ alignments (BC or AD). This scenario leads to the remarkable suggestion of rather extreme variations in crossing frequencies. For example, the observed crossings [25]) in the $\pi d_{5/2}$ ($\hbar\omega = 0.21$ MeV) and the $\pi h_{9/2}$ (0.40 MeV) bands of ^{185}Ir are both attributed to the AB alignment process, the large variation being due to large changes in γ.

Both scenarios of explaining the pattern of band crossings require further testing with new experiments. If the shape parameters really vary as much between configurations as the calculations predict, then lifetime measurements should be able to detect distinct $B(E2)$ changes before and after a band crossing. Measurements have been performed [47]) on the $[624]^{9+}_{\frac{1}{2}}$ band of ^{185}Pt, and the results should be able to help distinguish whether a $\nu i_{13/2}$ or $\pi h_{9/2}$ crossing occurs. Other important lifetime measurements are on ^{186}Pt, again to distinguish if the yrast crossing in the $\pi h_{9/2}$ band actually reduces the E2 strength.

Further spectroscopy measurements are also needed. The debate described here centers on whether the first band crossing in these nine nuclei is due to $\pi i_{13/2}$ or $\pi h_{9/2}$ alignment. Whichever is correct, the other should occur at a not too distant frequency. Most of the bands surveyed here are limited to data at $\hbar\omega < 0.4$ MeV. A survey of the range up to $\hbar\omega = 0.5$ MeV should produce more band crossings. The careful comparison of these anticipated crossings should be able to settle the question of how low in rotational frequency the $\pi h_{9/2}$ crossing can occur. Whatever the outcome of those future investigations, the current work has demonstrated the importance of combining detailed measurements on nuclei at high spins with careful calculations of the configuration-dependent shape of the nucleus.

Research at the University of Tennessee is supported by the U.S. Department of Energy under contract no. DE-FG05-87ER40361. Oak Ridge National Laboratory is operated by Martin Marietta Energy Systems Inc. under contract DE-AC05-84OR21400 with the U.S. Department of Energy. The Joint Institute for Heavy Ion Research is operated by the University of Tennessee, Vanderbilt University, and the Oak Ridge National Laboratory, and is supported by them and the DOE. This

work is supported in part by the Natural Sciences and Engineering Research Council of Canada, and the Swedish Natural Science Research Council.

References

1) S. Frauendorf and F.R. May, Phys. Lett. **B125** (1983) 245
2) R. Bengtsson, T. Bengtsson, J. Dudek, G. Leander, W. Nazarewicz and J.-Y. Zhang, Phys. Lett. **B183** (1987) 1, and references therein
3) A.J. Larabee, M.P. Carpenter, L.L. Riedinger, L.H. Courtney, J.C. Waddington, V.P. Janzen, W. Nazarewicz, J.Y. Zhang, R. Bengtsson and G. Leander, Phys. Lett. **B169** (1986) 21
4) L.L. Riedinger, V.P. Janzen and M.P. Carpenter, Proc. XXII Winter School on Physics, Zakopone, Poland, Part 1: Selected topics in nuclear structure, ed. by R. Broda and Z. Stachura (1987) p. 315
5) W. Nazarewicz, G.A. Leander and J. Dudek, Nucl. Phys. **A467** 437;
R. Bengtsson, T. Bengtsson, J. Dudek, G. Leander, W. Nazarewicz and J.-Y. Zhang, to be published
6) S. Pilotte, Etude de la déformation des noyaux de ^{185,186}Pt, Doctoral dissertation, Université de Montréal (1987)
7) J. Burde, R.M. Diamond and F.S. Stephens, Nucl. Phys. **A85** (1966) 481
8) M. Finger, R. Foucher, J.P. Husson, J. Jastrzebski, A. Johnson, G. Astner, B.R. Erdal, A. Kjelberg, P. Patzelt, A. Hoglund, S.G. Malmskog and R. Henck, Nucl. Phys. **A188** (1972) 369
9) M. Cailliau, R. Foucher, J.P. Husson and J. Letessier, J. de Phys. **35** (1974) 469
10) J. Burde, R.M. Diamond and F.S. Stepehsns, Nucl. Phys. **A92** (1967) 306
11) S. Beshai, K. Fransson, S. Hjorth, A. Johnson, T. Lindblad and J. Sztarkier, Z. Physik **A277** (1976) 351
12) C. Fahlander and G.D. Dracoulis, **A375** (1982) 263;
R.M. Lieder, G. Sletten, J. Borggreen and J. Pedersen, Nucl. Phys. **A375** (1982) 291
13) D. Popescu, W. Schmitz, J.K. Johansson, G. Kajrys, D.D. Rajnauth, J.C. Waddington, M.P. Carpenter, V.P. Janzen, L.L. Riedinger, S. Monaro and S. Pilotte, University of Tennessee Progress Report 88-03 (1988) 27;
W. Schmitz, Master's thesis, University of Bonn (1987)
14) R.M. Lieder, A. Neskakis, J. Skalski, G. Sletten, J.D. Garrett and J. Dudek, Nucl. Phys. **A476** (1988) 545
15) R. Bengtsson and S. Frauendorf, Nucl. Phys. **A327** (1979) 139
16) J. Nyberg, Studies of reaction mechanisms and nuclear structure in fusion-like heavy ion reactions, Doctoral dissertation, Royal Inst. of Technology, Stockholm, Sweden (1987);
J. Nyberg, A. Johnson, M.P. Carpenter, C.R. Bingham, L.H. Courtney, V.P. Janzen, S. Juutinen, A.J. Larabee, Z.-M. Liu, L.L. Riedinger, C. Baktash, M.L. Halbert, N.R. Johnson, I.Y. Lee, Y. Schutz, J. Waddington and D.G. Popescu, to be published
17) S. Pilotte, G. Kajrys, S. Monaro, M.P. Carpenter, V.P. Janzen, L.L. Riedinger, J.K. Johansson, D. Popescu, D.D. Rajnauth and J.C. Waddington, Phys. Rev. **C20** (1989) 610
18) V.P. Janzen, M.P. Carpenter, L.L. Riedinger, W. Schmitz, S. Pilotte, S. Monaro, D.D. Rajnauth, J.K. Johnansson, D.G. Popescu, J.C. Waddington, Y.S. Chen, F. Dönau and P.B. Semmes, Phys. Rev. Lett. **61** (1988) 2073
19) S. Frauendorf, L.L. Riedinger, J.D. Garrett, J.J. Gaardhøje, G.B. Hagemann and B. Herskind, Nucl. Phys. **A431** (1984) 511
20) A.C. Kahler, L.L. Riedinger, N.R. Johnson, R.L. Robinson, E.F. Zganjar, A. Visavanathan, D.R. Zolnowski, M.B. Hughes and T.T. Sugihara, Phys. Lett. **B72** (1978) 443
21) G. Hebbinghaus, W. Gast, A. Krämer-Flecken, R.M. Lieder, J. Skalski and W. Urban, Z. Phys. **A328** (1987) 387
22) P. Chowdhury, F. Azgui, S. Bjørnholm, J. Borggreen, C. Christenesen, B. Fabricius, A. Holm, J. Pedersen, G. Sletten, M. Bentley, D. Howe, R. Mokhtar, D. Morrison and J.F. Sharpey-Schaffer, Niels Bohr Institute Tandem Accelerator Laboratory Annual Report, 1987
23) K. Schiffer and J.D. Garrett, Proc. of the Int. Conf. on nuclear shapes, Crete, Greece (1987)

24) J.K. Johansson, D. Popescu, D.D. Rajnauth, J.C. Waddington, M.P. Carpenter, L.H. Courtney, V.P. Janzen, A.J. Larabee, Z.M. Liu and L.L. Riedinger, Phys. Rev. **C40** (1989) 132
25) D.L. Balabanski, W. Gast, G. Hebbinghaus, A. Krämer-Flecken, R.M. Lieder, T. Morek, T. Rzaca-Urban, H. Schnare and W. Urban, Z. Phys. **A332** (1989) 111;
S. André, J. Genevey-Rivier, J. Treherne, R. Kaczarowski, J. Lukasiak, J. Jastrzebski and C. Schück, Nucl. Phys. **A325** (1979) 445
26) V.P. Janzen, Z.M. Liu, M.P. Carpenter, L.H. Courtney, A.J. Larabee, L.L. Riedinger, J.K. Johnansson, D.G. Popsecu and J.C. Waddington, University of Tennessee Progress Report (1986) 36
27) A.J. Kreiner, J. Davidson, M. Davidson, P. Thieberger, E.K. Warburton, S. André and J. Genevey, Nucl. Phys. **A489** (1988) 525
28) C.H. Yu, private communication
29) J. Recht, Y.K. Agarwal, K.P. Blume, M. Guttormsen, H. Hübel, H. Kluge, K.H. Maier, A. Maj, N. Roy, D.J. Decman, J. Dudek and W. Nazarewicz, Nucl. Phys. **A440** (1985) 366
30) J. Espino, private communication
31) G.D. Dracoulis, P.M. Walker and A. Johnston, J. of Phys. **G4** (1978) 713
32) G.D. Dracoulis and P.M. Walker, Phys. Rev. **C20** (1979) 1619
33) R. Kulessa, R. Bengtsson, H. Bohn, H. Emling, T. Faestermann, F. von Feilitsch, E. Grosse, W. Nazarewicz, D. Schwalm and H.J. Wollersheim, unpublished
34) G. Dracoulis, C. Fahlander and M.P. Fewell, Phys. Rev. Lett. **45** (1980) 1831
35) A. Neskakis, R.M. Lieder, M. Muller-Veggian, H. Beuscher, W.F. Davidson and C. Mayer-Böricke, Nucl. Phys. **A261** (1976) 189
36) G.D. Dracoulis, A.E. Stuchbery, A.P. Byrne, A.R. Poletti, J. Ger and R.A. Bark, J. of Phys. **G12** (1986) L97
37) M.J.A. DeVoigt, R. Kaczarowski, H.J. Riezebos, R.F. Noorman, J.C. Bacelar, M.A. Deleplanque, R.M. Diamond, F.S. Stephens, J. Sauvage and B. Roussiere, submitted to Nucl. Phys. A
38) W. Nazarewicz, J. Dudek, R. Bengtsson, T. Bengtsson, and I. Ragnarsson, Nucl. Phys. **A435** (1985) 397;
S. Cwiok, J. Dudek, and W. Nazarewicz, to be published
39) J. Dudek, Z. Szymanski, and T. Werner, Phys. Rev. **C23** (1981) 920
40) W. Nazarewicz, Proc. Int. Conf. on nuclear shapes, Crete, Greece (1987)
41) U. Garg, A. Chaudhury, M. Drigert, E. Funk, J. Mihelich, D. Radford, H. Helppi, R. Holzmann, R. Janssens, T.L. Khoo, A.M. van den Berg and J.L. Wood, Phys. Lett. **B180** (1986) 319
42) W.C. Ma, A.V. Ramayya, J.H. Hamilton, S.J. Robinson, J.D. Cole, E.F. Zganjar, E.H. Spejewski, R. Bengtsson, W. Nazarewicz and J.Y. Zhang, Phys. Lett. **B167** (1986) 277
43) H. Hübel, A.P. Byrne, S. Ogaza, A.E. Stuchbery, G.D. Dracoulis and M. Guttormsen, Nucl. Phys. **A453** (1986) 316
44) F. Hannachi, G. Bastin, M.B. Porquet, C. Schück, J.P. Thibaud, C. Bourgeois, L. Hildingsson, D. Jerrestam, N. Perrin, H. Sergolle, F.A. Beck, T. Byrski, J.C. Merdinger and J. Dudek, Nucl. Phys. **A481** (1988) 135
45) F. Dönau, J.Y. Zhang, and L.L. Riedinger, Nucl. Phys. **A496** (1989) 333
46) J.Y. Zhang, F. Dönau, and L.L. Riedinger, to be published
47) L. Zhou, V.P. Janzen, H.Q. Jin L.L. Riedinger, N.R. Johnson, I.Y. Lee, F.K. McGowan, M.A. Riley, A. Virtanen, U. Garg, G. Kajrys, S. Monaro, N. Nadon and S. Pilotte, University of Tennessee Progress Report (1989) 14
48) R.B. Bengtsson in Proc. Conf. on contemporary topics in nuclear structure, Cocoyoc, Mexico, June 9-14, 1988